Archive of Applied Mechanics (2023) 93:261–286
https://doi.org/10.1007/s00419-022-02170-w

ORIGINAL

Wei Ding · John P. Hollkamp · Sansit Patnaik · Fabio Semperlotti

On the fractional homogenization of one-dimensional elastic metamaterials with viscoelastic foundation

Received: 1 November 2021 / Accepted: 26 April 2022 / Published online: 18 May 2022

Abstract This work investigates the application of space–time fractional-order operators to the simulation of linear elastic waves propagating in 1D periodic structures resting on a viscoelastic foundation. More specifically, this study focuses on the possible application of fractional-order mathematics as the foundation to develop efficient reduced-order models capable of capturing the wave dynamics in periodic, viscoelastic one-dimensional metamaterials. By leveraging a space–time fractional formulation of the wave equation, we develop a homogenized model capable of capturing either material or geometric inhomogeneity and viscoelastic behavior. First, we derive the dispersion relation for a 1D infinite periodic bar resting on a longitudinal viscoelastic foundation using integer order formulation, which serves as a reference point in this work. Then, we obtain the dispersion relationships associated with two different fractional formulations. The first formulation relies on the use of time-fractional derivatives and focuses on capturing the dissipation induced by the viscoelastic foundation. The second formulation relies on the use of space–time fractional derivatives in order to lead to a homogenized one-dimensional model of the periodic bar. In order to achieve real-valued fractional orders, a matching approach between the dispersion relations of the fractional- and integer-order differential equations is used. Numerical simulations show that the space–time fractional wave equation serves as an effective homogenized model that well represents the wave propagation in a 1D periodic bar on a viscoelastic foundation. The results also illustrate that the use of space-fractional derivatives allows modeling the dynamics within (low order) frequency band gaps, a result typically not achievable with classical homogenization techniques.

Keywords Periodic structures · Viscoelastic foundations · Homogenization · Fractional calculus

List of symbols

ρ_i	Mass density for material i
$\hat{\rho}_i$	Effective mass density for material i in time-fractional wave equation
$\hat{\rho}$	Effective mass density in space–time fractional wave equation
E_i	Young's modulus for material i
$\hat{E}$	Effective Young's modulus in space–time fractional wave equation

Supplementary Information The online version contains supplementary material available at https://doi.org/10.1007/s00419-022-02170-w.

W. Ding (✉) · J. P. Hollkamp · S. Patnaik · F. Semperlotti (✉)
Department of Mechanical Engineering, Ray W. Herrick Laboratories, 177 S. Russell St., West Lafayette, IN 47907, USA
E-mail: ding242@purdue.edu

F. Semperlotti
E-mail: fsemperl@purdue.edu

L_i	Length of material i within the unit cell
Δ_{L}	Length of the unit cell
A	Cross-sectional area
k	Elastic stiffness parameter of the viscoelastic foundation
c	Damping parameter of the viscoelastic foundation
$\overline{k}$	Effective elastic stiffness parameter of the viscoelastic foundation
$\overline{c}$	Effective damping parameter of the viscoelastic foundation
μ	Wavenumber in integer-order Bloch wave solution
$\tilde{\mu}$	Wavenumber in time-fractional Bloch wave solution
$\tilde{\tilde{\mu}}$	Wavenumber in space–time fractional Bloch wave solution
f	Frequency
ω	Angular frequency
$\Re(\cdot)$	Real component
$\Im(\cdot)$	Imaginary component
u_i	Integer-order Bloch wave solution for material i
$\tilde{u}_i$	Time-fractional Bloch wave solution for material i
$\tilde{\tilde{u}}$	Space–time fractional Bloch wave solution
U_i	Periodic function defined in integer-order Bloch wave solution for material i
$\tilde{U}_i$	Periodic function defined in time-fractional Bloch wave solution for material i
$\tilde{\tilde{U}}$	Amplitude in space–time fractional Bloch wave solution
λ_i	Exponent defined in integer-order Bloch wave solution for material i
$\tilde{\lambda}_i$	Exponent defined in time-fractional Bloch wave solution for material i
β_i	Time-fractional order for material i in time-fractional wave equation
α	Space-fractional order in space–time fractional wave equation
β	Time-fractional order in space–time fractional wave equation

1 Introduction

The rapid advancements in additive manufacturing techniques have further focused on the attention of the engineering community on the design and analysis of complex heterogeneous structures with non-trivial geometries. To date, many examples of architectured structures exploit either the periodic gradation of materials or of geometric structural features to tailor the dynamic behavior [1–5]. In the case of periodic structures, systems are assembled by repeating periodically in space a fundamental unit cell that captures in itself all the distinctive constitutive material and geometric features of the overall structure. The properties of the unit cell can be designed to enable the periodic structure to exhibit unique wave-guiding characteristics including wave shaping, collimation, focusing, and steering [4–9]. These remarkable properties of periodic structures have resulted in a wide range of applications in the most diverse fields of engineering, nanotechnology, and even biotechnology. Specific examples of applications of periodic structures include biological implants and wearable devices [10,11], micro/nano-electromechanical devices [7,8,12], and even macroscale structures relevant to aerospace, railway, and civil engineering applications [13–16].

In several of the aforementioned examples, the heterogeneous structures are often accompanied by elastic and viscoelastic elements that further the ability to tailor its wave-guiding characteristics. As an example, the soft filaments used in solid-propellant rocket motors [13], the ballast underlying railway tracks, foundations of buildings and off-shore pipelines [15–17], the cushioning and air gaps used in performance footwear, and even the foundation structure of most biological implants [10,11,18] can be abstracted and analyzed as either elastic or viscoelastic foundations that when combined with the heterogeneous parent structure could be designed potentially to achieve vibration and shock control and stress wave propagation. Indeed, the interplay between periodic structures and structural foundations in these types of applications adds more flexibility to the design and creates new degrees of freedom to control the overall dynamics. In all these applications, the ability to develop accurate and computationally efficient models is paramount to achieving the full performance potential.

During the past few decades, several analytical and numerical approaches have been proposed to simulate the dynamics of periodic structures on different types of foundations. Based on the underlying physical model and the numerical technique adopted to simulate the model, the most established approaches could be broadly classified into five categories: discrete approaches, classical homogenization approaches, asymptotic approaches, computational homogenization approaches, and nonlocal homogenization approaches. We

briefly review these approaches in the following section. The key highlights of the different approaches, their advantages, and the challenges faced by them are summarized in the following:

- *Discrete approaches* are invariably based on the classical (local) approach to continuum mechanics. From a high-level perspective, these approaches are characterized by a process of discretization of the system in space and/or time, or discretization of the system response in terms of appropriately chosen test functions. Examples of the former approach include finite difference methods [19] and finite element methods [20], while examples of the latter approach include plane-wave expansion methods [21] and variational methods [22]. These techniques have found good success and are still widely used, but they are subject to an implicit trade-off between computational time and prediction accuracy (that is directly related to the resolution of the specific approach). Additionally, for structures with multiscale spatial inhomogeneity or memory effects, discrete methods require very fine resolution to capture accurately the multiscale response and lead rapidly to computational resources that are beyond available capabilities. This is often encountered in the simulation of porous, polymeric, and functionally graded materials [18,23,24].
- *Classical homogenization approaches* eliminate the spatial variation of the material and geometric parameters typical of heterogeneous structures by replacing them with so-called effective parameters, that is spatially independent (constant) parameters capable of representing the behavior of the original structure in an approximate sense [25,26]. These homogenized (or effective) properties facilitate the use of classical continuum theory for the simulation of the response of these complex media. While homogenization approaches offer a powerful alternative that is not subject to the same computational cost of discrete methods, classical homogenization approaches encounter some important limitations when applied in a dynamic regime. The homogenized material properties can be representative of the actual heterogeneous medium only when the wavelength of the propagating wave is sufficiently larger than the characteristic length scales of the microstructural features. This limits their application to the low-frequency regime and does not allow classical homogenization approaches to predict the existence of frequency band gaps [27,28].
- *Asymptotic approaches* use either multiscale expansions of bulk (homogenized) material properties in the spatial domain or perturbation of homogenized response fields in the temporal domain to capture some aspects of microstructural features and memory effects. Examples of asymptotic methods used for the analysis of complex structures include high-frequency homogenization that is used for spatial homogenization of periodic structures [27,29], as well as higher-order averaging, incremental harmonic balance, and multiple scales analysis [11,16,30] which are typically used to capture memory effects across different temporal scales. Very recently, advanced asymptotic homogenization techniques have been developed to model complex hierarchical biological structures [31–33] and nonlinear heterogeneous materials [34,35]. Despite providing a very successful approach to broadband homogenization, a major limitation of asymptotic methods follows from the rather complex analytical derivation that is only viable for limited types of structural analysis (and under specific loading conditions). In the context of the present study, we also note that comprehensive models capable of combining asymptotic methods in both space and time (necessary to analyze periodic structures on viscoelastic foundations) appear to be absent in the literature.
- *Computational homogenization approaches* construct a microscale boundary value problem to capture the influence of the microstructure at the continuum (macroscopic) level [36]. Along with the development of computational methods, in the past 2 decades, computational homogenization has received increasing attention. Examples include, but are not limited to, finite element-based [37,38], FFT-based [39,40], and even data-driven [41,42] computational homogenization techniques. While this class of homogenization approaches can well capture the multiscale behavior, the strong coupling between computational methods and homogenization indicates that these approaches are still computationally expensive [32].
- *Nonlocal homogenization approaches* based on fractional-order calculus have been recently used to model the response of heterogeneous periodic media as well as viscoelastic media [28,43–47]. Fractional-order operators enable the differentiation and integration to any real or complex order, are intrinsically multiscale, and provide a natural way to account for several complex physical mechanisms such as nonlocal effects [45,48–50], medium heterogeneity [51,52], and memory effects [53–56]. While time-fractional operators enable memory effects (i.e., the response of a system is a function of its past history), space-fractional operators can account for medium heterogeneity and nonlocal effects. In other terms, while temporal fractional derivatives physically represent damping and dissipation that occur in lossy or viscoelastic materials [57–59], spatial fractional derivatives are indicative of attenuation in systems that potentially are still conservative [28,44]. In other terms, space-fractional derivatives are ideal tools to capture frequency band gaps in which attenuation is due to multiple back scattering and not to energy dissipation. Indeed, this latter concept was leveraged in previous studies [28,44–46] to obtain the homogenized equations governing

the dynamic response of periodic structural elements. One of the most notable results of these studies was the observation of the validity of the fractional homogenized equations beyond the classical homogenization limit and their ability to capture the response within (low order) frequency band gaps. Remarkably, unlike discrete approaches, fractional calculus-based nonlocal homogenization approaches are often associated with lower computational cost [23,24,28]. This discussion suggests that fractional calculus can serve as a powerful mathematical tool for the homogenization and analysis of dissipative periodic structures, such as periodic systems resting on viscoelastic foundations. In this regard, we note that a comprehensive space–time fractional homogenized formulation capable of modeling periodic structures with dissipation is still missing. Finally, we note that the formulation developed in [28,43] resulted in complex-valued fractional orders that renders the model sensitive to numerical approximations adopted in the evaluation of complex-order fractional operators. A method capable of casting the homogenized problem in terms of only real-valued fractional orders would greatly benefit accuracy and efficiency.

While the above discussion is not meant to provide a comprehensive overview of the broad topic of computational methods for periodic systems, it does highlight some key limitations of these established methodologies. From the above discussion, we conclude that existing approaches are not theoretically and computationally equipped to provide a comprehensive and simultaneous account of spatial and temporal attenuation that can occur in the response of dissipative periodic structures, such as those connected to elastic and viscoelastic foundations. However, fractional calculus-based approaches present the most promising route in terms of the range of validity, accuracy, and potential computational efficiency to model the different physical mechanisms underlying the response of periodic and lossy structures.

In this study, we leverage fractional calculus to develop a comprehensive temporal and spatial homogenization approach. More specifically, we extend the previously developed space-fractional approaches [28] to time- and space-fractional approaches that simulate the response of periodic structures on viscoelastic foundations. The coexistence of Bragg scattering resulting from material periodicity and the viscoelastic effects from the foundation can be simultaneously captured by space- and time-fractional operators, respectively. Moreover, by deriving real-valued fractional model parameters, the proposed method will address numerical instabilities characteristic of previously developed fractional-order approaches. The overall contributions of this study are threefold:

- *To formulate a reference one-dimensional periodic system on a foundation* we consider a bi-material periodic rod resting on a viscoelastic foundation. In the following, we will refer to the periodic rod on the foundation as the "periodic system," for the sake of brevity. The viscoelastic foundation is idealized by means of lumped spring and damper elements operating in parallel; this simple modeling assumption allows easily exploring the range of possible foundation conditions (from purely elastic to purely viscous). First, the classical integer-order governing equations describing the periodic system are derived and their analytical dispersion relations are presented. The analytical solutions of the fully resolved integer-order model provide the reference solution to validate the prediction obtained from the fractional-order homogenized model. Further, the dispersion relations will be used to derive the fractional model parameters.
- *To develop a time-fractional order homogenization approach* we develop a reduced-order model that captures the impact of the viscoelastic foundation on the bi-material periodic bar by using time-fractional operators. By leveraging the memory effect of time-fractional derivative, we propose a periodic time-fractional wave equation that allows to capture the ultra-low band gap as well as damping effect brought by external viscoelastic forces.
- *To develop a space–time fractional-order homogenization approach* we further homogenize the bi-material periodic bar in the second step using space-fractional operators to capture the spatial heterogeneity and its impact on the system dynamics. Specifically, we further extend the periodic time-fractional wave equation obtained in the first step into the homogeneous space–time fractional-order wave equation. While the time-fractional operators capture the viscoelastic effects, the space-fractional operators, at the same time, are leveraged to capture wave propagation characteristics due to material periodicity.

Note that in each fractional-order homogenization step, the homogenization, or the dynamic equivalence between the original integer model and the fractional models, is achieved by matching dispersion relations. Specifically, we derive the dispersion characteristics of the corresponding fractional-order elastodynamic equations and compare them directly to the dispersion relations derived from the integer-order model. This enables an inverse strategy to determine the fractional model parameters. We highlight that the strategy to determine the model parameters in a fractional model can follow different avenues such as: **(T1)** matching techniques based on representative system characteristics (in the case of this study, the dispersion properties)

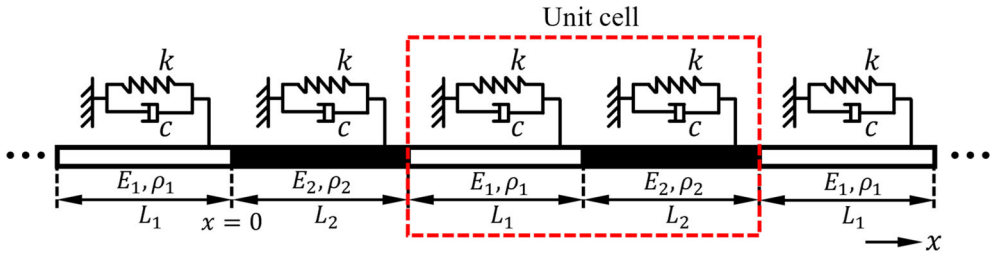

Fig. 1 Schematic showing the configuration of a 1D bi-material bar on a longitudinal viscoelastic foundation. The bar is composed of periodic sections made of two different materials. Sections containing material 1 and material 2 are distinguished using white and black colors. For each material $i = 1, 2$, E_i is Young's modulus, ρ_i is density, and L_i is length of material section. The evenly distributed longitudinal viscoelastic foundation is illustrated using Kelvin–Voigt model. The elastic effect is represented using springs with stiffness k and the damping is represented using dampers with damping coefficient c

[28,43]; **(T2)** derivation of physics-driven laws [60,61]; and **(T3)** data-driven techniques [23,51,62], depending on the underlying physics being captured. Broadly speaking, matching techniques are suitable when fractional calculus is employed to simplify models while maintaining accuracy (e.g., fractional homogenization and model-order reduction, like in the present study). In the case of evolutionary nonlinear problems, such as contact dynamics [60], viscoelastic mechanics [63], and dynamic fracture [61], physics-driven laws could be defined and embedded in the order definition so as to determine the order variation based on the instantaneous response of the system. Finally, to describe physical mechanisms that are intrinsically fractional and, as such, not fully described by integer-order operators (e.g., anomalous and hybrid transport processes), data fitting selected characteristics of fractional models against experimentally obtained data becomes an indispensable tool. Typically used approaches in this latter category include standard regression techniques [56,57] and even machine learning techniques [23,64,65]. While there is a lack of widespread consensus on general inverse methods, the inverse strategy adopted here does not have any bearing on the generality of the fractional-order homogenization technique, developed in this study for periodic systems.

Before proceeding further, we emphasize that the periodic bar system was chosen in order to enable a clear and more transparent development of the fractional-order homogenized model since it enables analytical approaches to obtain the dispersion relations (required for the inverse problem) and the system response from the governing equations (required for validation) for both the integer- and fractional-order models. However, the overall time- and space-fractional model development strategy, the inverse strategy, and the validation procedure are highly general in nature and can be extended to other periodic structural elements on viscoelastic foundations.

The remainder of this paper is structured as follows: First, we derive the dispersion relation and the analytical solution of the integer-order governing equations that describe the response of the periodic system in Sect. 2. Then, in Sect. 3, we develop the fractional-order homogenized models and determine the fractional model parameters. Finally, in Sect. 4 we validate the fractional-order homogenized model via direct numerical simulations and also explore the ultra-low-frequency band gap as well as the dissipating characteristics of periodic bars attached to elastic foundations.

2 Periodic bar on a viscoelastic foundation: integer-order formulation

In this section, we first present a periodic 1D bi-material bar structure with a longitudinal viscoelastic foundation as shown in Fig. 1. To determine the fractional model parameters of the corresponding effective model, we derive the governing equations and the dispersion relationship describing the wave propagation through this structure using a fully resolved integer-order formulation.

2.1 Governing integer-order equations and dispersion relation

We consider an infinite bi-material periodic bar resting on a viscoelastic foundation, as shown in Fig. 1. As illustrated in Fig. 1, the periodic bar consists of two sections and the viscoelastic foundation has uniform properties throughout the length of the bar. The length of the two sections within the periodic bar are denoted as L_1 and L_2, such that the lattice constant of the bar is $\Delta_{\mathrm{L}} = L_1 + L_2$. The coordinate system is chosen such

that the origin coincides with the interface of the two sections (see Fig. 1). It follows that section #1 appears for $x \in [-L_1 + N\Delta_L, N\Delta_L]$, while section #2 appears for $x \in [N\Delta_L, L_2 + N\Delta_L]$, where N is the set of integers and x is the spatial location along the length of the bar. Further, the elastic modulus, density, and cross-sectional area of each section are assumed to be homogeneous and are indicated as E_i, ρ_i, and A_i with $i \in \{1, 2\}$, respectively.

In the classical locally elastic description, the governing equation of a heterogeneous bar resting on a heterogeneous viscoelastic foundation is expressed using integer-order differential operators as [28]:

$$\frac{\partial^2 u(x,t)}{\partial t^2} + \left[\frac{c(x)}{\rho(x)}\right]\frac{\partial u(x,t)}{\partial t} + \left[\frac{k(x)}{\rho(x)}\right]u(x,t) = \frac{1}{\rho(x)}\frac{\partial}{\partial x}\left[E(x)A(x)\frac{\partial u(x,t)}{\partial x}\right] \tag{1}$$

where $u(x,t)$ denotes the axial displacement of the bar at the spatial location x and time instant t. Further, $E(x)$, $\rho(x)$, and $A(x)$ denote the Young's modulus, density, and cross-sectional area of the heterogeneous bar, respectively. Similarly, $k(x)$ and $c(x)$ denote the stiffness and viscous damping coefficients of the heterogeneous foundation. For the periodic bar introduced previously in this section, the Young's modulus and density are both periodic functions with a spatial period $\Delta_L (= L_1 + L_2)$, and the cross-sectional area is assumed uniform across the length of the bar (that is, $A(x) = A$). Further note that, within each section of the bar, both material and geometric properties are uniform. Finally, for the homogeneous viscoelastic foundation, the elastic and damping properties are constant functions in space, that is, $k(x) = k$, and $c(x) = c$. Following the above assumptions, we simplify the governing equation provided in Eq. (1) to the following version that is applicable to each individual section of the bar:

$$\frac{\partial^2 u_i}{\partial t^2} + \frac{\overline{c}}{\rho_i}\frac{\partial u_i}{\partial t} + \frac{\overline{k}}{\rho_i}u_i = \frac{E_i}{\rho_i}\frac{\partial^2 u_i}{\partial x^2} \tag{2}$$

where $i = 1\ \forall\ x \in [-L_1 + N\Delta_L, N\Delta_L]$ and $i = 2\ \forall\ x \in [N\Delta_L, L_2 + N\Delta_L]$. Further, we have denoted c/A and k/A as $\overline{c}$ and $\overline{k}$, respectively. Henceforth, in the interest of a more compact notation, we will not explicitly denote the functional dependence of the axial displacement on the spatial and temporal variables.

2.2 Dispersion relation

In this section, we obtain the dispersion relation for the system discussed in the previous section. Broadly speaking, the dispersion relations can be derived by assuming either (1) a real-valued wavenumber and deriving the corresponding complex angular frequency or (2) a real-valued frequency and deriving the corresponding complex wavenumber [66,67]. While the former approach enables capturing transient decay (via the imaginary component of the frequency) in amplitudes typical of free vibrations of damped systems, the latter approach is more suitable in capturing spatial decay (via the imaginary component of the wavenumber) resulting from multiple scattering in forced systems. Examples of the two approaches can be found in [68–70]. In this study, we primarily consider the latter approach to analyze the spatially damped time-harmonic waves in the periodic system. For this purpose, we first assume a time-harmonic solution for the axial displacement u_i of each section within the bar. Next, the periodic nature of the coefficients in the governing differential equation of the bar (resulting from the periodic variation in the bar properties) allows using Floquet theorem to describe the spatial displacement as a quasi-periodic function across adjoining unit cells [71]. Consequently, the axial displacement of each section within the bar can be assumed given by:

$$u_i(x,t) = U_i(x)\mathrm{e}^{\mathrm{j}\mu x}\mathrm{e}^{\mathrm{j}\omega t} \tag{3}$$

where U_i denotes the amplitude of section i. Given the quasi-periodic nature of the axial displacement, the amplitude is a periodic function such that $U_i(x) = U_i(x + \Delta_L)$. Note, this latter expression also ensures consistency of the displacement field at the interface between two adjoining unit cells within the bar. Further, in Eq. (3), $\mathrm{j} = \sqrt{-1}$ denotes the imaginary number, and μ and ω denote the Floquet wavenumber and the angular frequency, respectively. Note that as we previously clarified, both μ and ω can be complex-valued to capture spatial attenuation and temporal dissipation of the axial response of the beam, respectively.

By substituting the ansatz in Eq. (3) into Eq. (2), we obtain the following governing equation describing the spatial variation of the amplitude U_i:

$$\frac{\partial^2 U_i}{\partial x^{*2}} + 2\mathrm{j}\mu\frac{\partial U_i}{\partial x^*} + \left[(\mathrm{j}\mu)^2 - \frac{\overline{k}}{E_i} - \frac{\mathrm{j}\omega\overline{c}}{E_i} - \frac{(\mathrm{j}\omega)^2\rho_i}{E_i}\right]U_i = 0 \tag{4}$$

where for convenience, we use x^* to represent the relative position of x within the current periodic interval. The relation between x^* and x is given as $x^* = x - N\Delta_\mathrm{L}\ \forall\, x \in [-L_1 + N\Delta_\mathrm{L}, L_2 + N\Delta_\mathrm{L}]$. The solution of the above second-order ordinary differential equation is obtained as:

$$U_i(x) = U_{i1}\mathrm{e}^{(\lambda_i - \mathrm{j}\mu)x^*} + U_{i2}\mathrm{e}^{(-\lambda_i - \mathrm{j}\mu)x^*} \tag{5}$$

where U_{i1} and U_{i2} are either real or complex constants. Further, μ_i is given as:

$$\lambda_i = \sqrt{\frac{\overline{k}}{E_i} + \frac{\mathrm{j}\omega\overline{c}}{E_i} + \frac{(\mathrm{j}\omega)^2\rho_i}{E_i}} \tag{6}$$

Note that unlike $u_i(x)$ in Eq. (3), the solution to $U_i(x)$ in Eq. (5) is periodic in nature. Substituting Eq. (5) back into Eq. (3), the overall displacement field in the periodic bar can now be expressed as:

$$u_i(x,t) = U_{i1}\mathrm{e}^{(\lambda_i - \mathrm{j}\mu)x^*}\mathrm{e}^{\mathrm{j}\mu x}\mathrm{e}^{\mathrm{j}\omega t} + U_{i2}\mathrm{e}^{(-\lambda_i - \mathrm{j}\mu)x^*}\mathrm{e}^{\mathrm{j}\mu x}\mathrm{e}^{\mathrm{j}\omega t} \tag{7}$$

The dispersion relations for the periodic bar can be derived by establishing a relationship between the set of four constants U_{i1} and U_{i2}. Imposing the continuity of displacement and axial force at the interface of the two sections (that is, at $x = 0$) results in the following set of two equations:

$$u_1(0) = u_2(0) \tag{8a}$$

$$E_1\frac{\partial u_1}{\partial x}\bigg|_{x=0} = E_2\frac{\partial u_2}{\partial x}\bigg|_{x=0} \tag{8b}$$

An additional set of two equations are established below by using the Floquet theorem in order to relate the displacement and axial force at $x = -L_1$ and at $x = L_2$:

$$u_1(-L_1) = u_2(L_2)\mathrm{e}^{\mathrm{j}\mu\Delta_\mathrm{L}} \tag{9a}$$

$$E_1\frac{\partial u_1}{\partial x}\bigg|_{x=-L_1} = E_2\frac{\partial u_2}{\partial x}\bigg|_{x=L_2}\mathrm{e}^{\mathrm{j}\mu\Delta_\mathrm{L}} \tag{9b}$$

By using the displacement field solution in Eq. (7) within the above-provided set of continuity conditions, we obtain the following algebraic set of equations:

$$\begin{bmatrix} 1 & 1 & -1 & -1 \\ E_1\lambda_1 & -E_1\lambda_1 & -E_2\lambda_2 & E_2\lambda_2 \\ \mathrm{e}^{-\lambda_1 L_1 + \mathrm{j}\mu\Delta_\mathrm{L}} & \mathrm{e}^{-\lambda_1 L_1 + \mathrm{j}\mu\Delta_\mathrm{L}} & -\mathrm{e}^{\lambda_2 L_2} & -\mathrm{e}^{-\lambda_2 L_2} \\ E_1\lambda_1\mathrm{e}^{-\lambda_1 L_1 + \mathrm{j}\mu\Delta_\mathrm{L}} & -E_1\lambda_1\mathrm{e}^{-\lambda_1 L_1 + \mathrm{j}\mu\Delta_\mathrm{L}} & -E_2\beta_2\mathrm{e}^{\lambda_2 L_2} & E_2\lambda_2\mathrm{e}^{\beta_2 L_2} \end{bmatrix} \begin{bmatrix} A_1 \\ B_1 \\ A_2 \\ B_2 \end{bmatrix} = 0 \tag{10}$$

For a nontrivial solution to the displacement field of the periodic beam the determinant of the coefficient matrix in Eq. (10) must be set to zero. This yields the dispersion relation for the periodic bar as:

$$\cos(\mu\Delta_\mathrm{L}) = \cos(\mathrm{j}\lambda_1 L_1)\cos(\mathrm{j}\lambda_2 L_2) - \frac{1}{2}\sin(\mathrm{j}\lambda_1 L_1)\sin(\mathrm{j}\lambda_2 L_2)\left(\frac{E_1\lambda_1}{E_2\lambda_2} + \frac{E_2\lambda_2}{E_1\lambda_1}\right) \tag{11}$$

The roots of the above nonlinear equation, for a given value of ω, give the value of the Floquet wavenumber μ. More specifically, we have:

$$\mu = \frac{1}{\Delta_\mathrm{L}}\cos^{-1}\left[\cos(\mathrm{j}\lambda_1 L_1)\cos(\mathrm{j}\lambda_2 L_2) - \frac{1}{2}\sin(\mathrm{j}\lambda_1 L_1)\sin(\mathrm{j}\lambda_2 L_2)\left(\frac{E_1\lambda_1}{E_2\lambda_2} + \frac{E_2\lambda_2}{E_1\lambda_1}\right)\right] + \frac{2\pi M}{\Delta_\mathrm{L}} \tag{12}$$

where M is the set of integers and $\cos^{-1}(\cdot)$ is the inverse cosine function. Without any loss of generality, we choose $M = 0$ here by taking the principal value of the inverse cosine function. This latter choice merely results in a folding of the dispersion curves across the irreducible part of the first Brillouin zone of the periodic bar (as also evident from the results presented later in this section). In the absence of the viscoelastic foundation (that is, $\overline{k} = \overline{c} = 0$), Eq. (11) reduces to the dispersion relation of an elastic bi-material periodic bar [29]. Similar to the case where $\overline{k} = \overline{c} = 0$, the real ($\Re(\mu)$) and the complex ($\Im(\mu)$) part of the wavenumber capture the wave oscillation and wave attenuation, respectively [28,29]. By using the complex wavenumber approach,

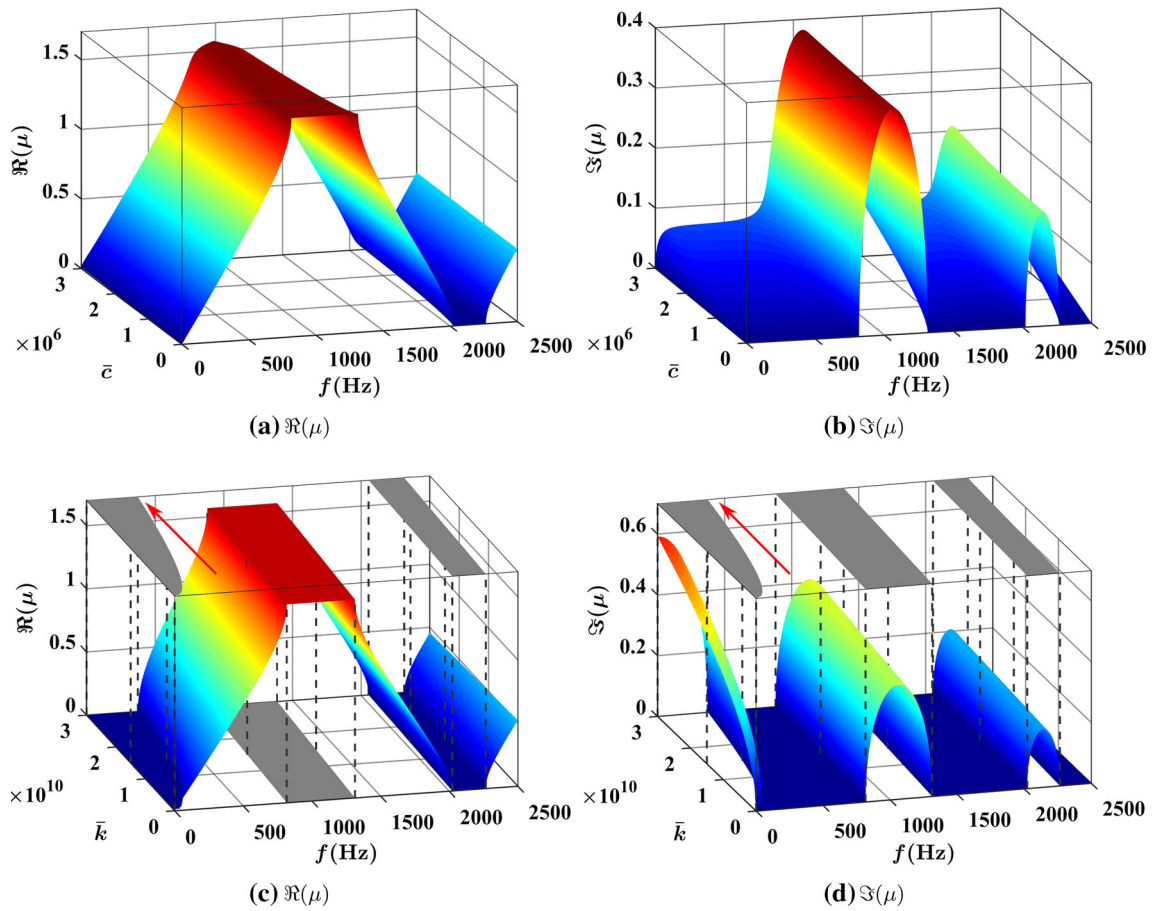

(a) $\Re(\mu)$ **(b)** $\Im(\mu)$ **(c)** $\Re(\mu)$ **(d)** $\Im(\mu)$

Fig. 2 3D plots showing the evolution of the dispersion curves for the 1D bi-material periodic bar on a viscoelastic foundation. **a** and **b** show how the dispersion relations evolve with the characteristics of the viscous foundation ($\bar{c} \in [0, 3 \times 10^6]$ and $\bar{k} = 0$); **c** and **d** show how the dispersion relations evolve with the characteristics of the elastic foundation ($\bar{k} \in [0, 3 \times 10^{10}]$ and $\bar{c} = 0$). It can be observed that (1) the viscous foundation mainly affects $\Im(\mu)$ such that the wave will become evanescent at all frequencies, and (2) the elastic foundation mainly affects the dispersion at ultra-low frequencies by creating an additional band gap. The evolution of the three band gaps is explicitly illustrated in (**c**) and (**d**) by projecting on the top and bottom planes using three shaded gray regions. The left shaded region is the ultra-low band gap created by the elastic foundation and the middle and right shaded regions are the band gaps created by material periodicity. Red arrow lines indicate the growth of the ultra-low band gap size with the elastic constant $\bar{k}$. (Color figure online)

Eq. (12) is derived to represent a solution for steady-state elastic waves [29]. Note that while other approaches such as complex frequency and even complex wavenumber/frequency formulation can be used [68–70] are also available for deriving dispersion relations, they are more suitable for analyzing transient waves (or free wave dissipation) in periodic structures, not for analyzing steady-state waves. Moreover, unlike the complex frequency approach which requires solving the nonlinear dispersion relation equation in Eq. (11), the same dispersion relation equation can be easily solved via inverse cosine function using the complex wavenumber approach. We remark that despite the different available approaches, the overall purpose (developing fractional homogenized model) as well as the physical mechanism (the dispersion relation) in this study should remain unchanged; hence, these approaches (that are used to derive dispersion relations) do not alter the overall framework of the inverse strategy.

In the subsequent analysis, we consider a periodic bar consisting of two alternating materials. The corresponding mechanical properties of the two sections are $E_1 = 70$ GPa, $\rho_1 = 2700$ kg/m^3 (consistent with aluminum) and $E_2 = 110$ GPa, $\rho_2 = 8100$ kg/m^3 (consistent with brass). Each section is assumed to have equal length $L_1 = L_2 = 1$ m. The dispersion relation in Eq. (12) can be used to obtain some qualitative insights on the effect of the viscoelastic foundation on the behavior of the periodic bar. For this purpose, we performed two independent parametric studies. *Study 1*: we set $\bar{k} = 0$ and analyze the impact of $\bar{c}$; and *Study 2*:

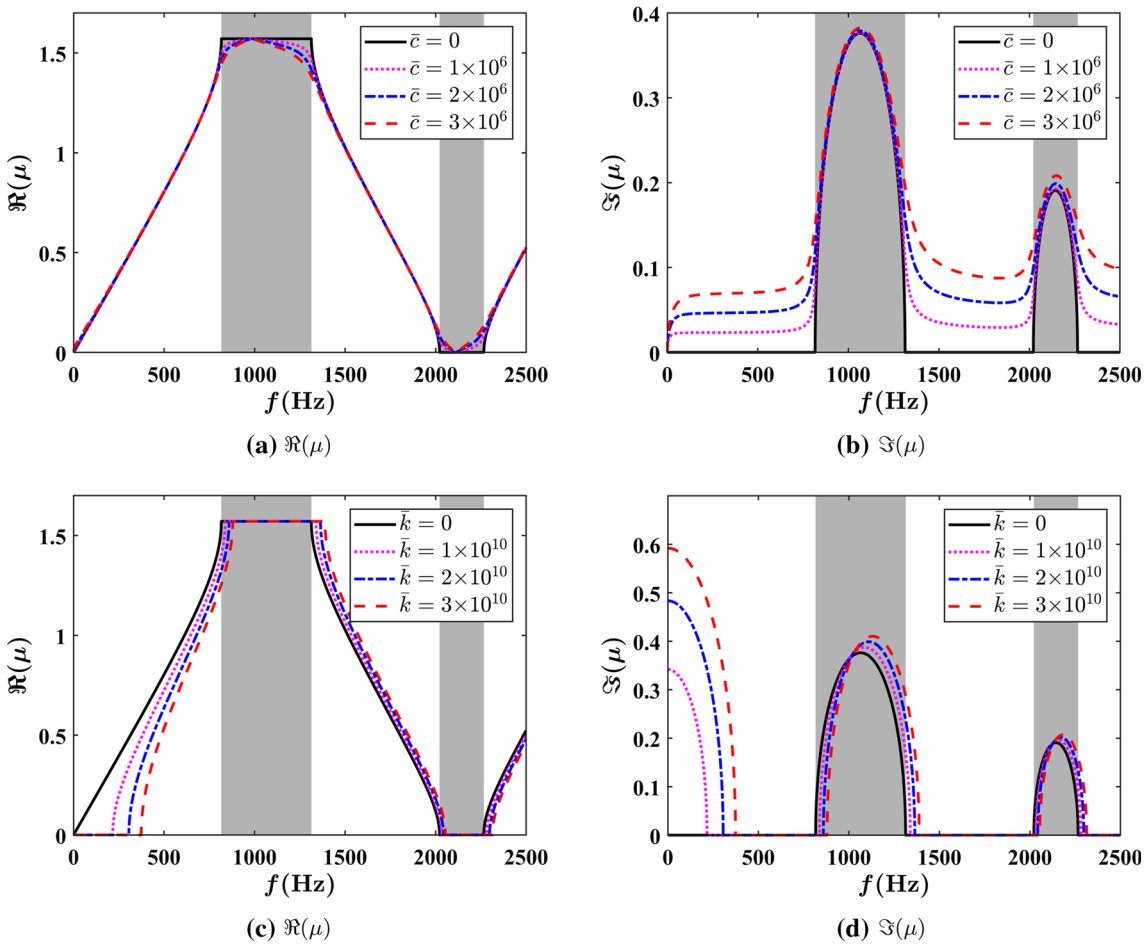

Fig. 3 2D plots of dispersion curves for the 1D bi-material periodic bar on a viscoelastic foundation. **a** and **b** show how the dispersion relation changes in study 1 (with $\bar{c}$ varying and $\bar{k} = 0$); **c** and **d** show how dispersion relation changes in study 2 (with $\bar{k}$ varying and $\bar{c} = 0$). It can be observed that when without viscoelastic foundation (both $\bar{k} = 0$ and $\bar{c} = 0$), band gaps shown by the two gray regions (same for other figures in this study) exist approximately in frequency interval [800 Hz, 1300 Hz] and [2000 Hz, 2300 Hz], in agreement with the results obtained in [28]. Band gaps of periodic bars with no viscoelastic foundation (that is, $\bar{k} = 0$ and $\bar{c} = 0$) are highlighted with gray colored regions

we set $\bar{c} = 0$, and analyze the impact of $\bar{k}$. The results of these studies are presented in Figs. 2 and 3. Note that the 3D plots in Fig. 2 are presented to show the detailed evolution of the dispersion curves with continuously distributed values of $\bar{k}$ and $\bar{c}$. The 2D plots in Fig. 3 are presented to show the dispersion relations for selected values of $\bar{k}$ and $\bar{c}$ (see legends in Fig. 3 for those values). Also note that, unlike the shaded regions in the 3D plots that help understanding the evolution of the band gaps (the shaded regions are not shown in the case of $\bar{c} \neq 0$ where $\Im(\mu) > 0$ at all frequencies so the band gaps do not exist), the shaded regions in the 2D plots only represent the band gaps of the periodic bars without viscoelastic foundation; this serves as a reference to identify variations in the dispersion curves. In order to better illustrate the dispersion relations as well as the wave propagation behavior, we use $f = \omega/2\pi$ (in the unit Hz) in all the plots to denote the frequency.

A detailed analysis of the results corresponding to the parametric studies leads to the following observations:

- As evident from the results presented in Figs. 2a, b and 3a, b, the existence of a viscous foundation leads to energy dissipation which results in a nonzero value of $\Im(\mu)$ at all frequencies. As $\bar{c}$ increases for a given frequency f, the dissipation effect becomes stronger, and thus $\Im(\mu)$ also increases at the specific f. This characteristic can be explicitly observed in Fig. 3b. Recall that this latter phenomenon is different from spatial attenuation (which is a conservative phenomenon) and it results in a reduction in size of the band gap (which is connected to spatial attenuation). This latter behavior is consistent with the nature of lossy metamaterials as extensively presented in the literature [3,56,57].

- The existence of the elastic foundation in the absence of damping (that is $\overline{c} = 0$) results in the occurrence of a very low-frequency band gap that can potentially shift down to zero frequency (see Figs. 2c, d and 3c, d). In Sect. 4, we will numerically validate the occurrence of the low-frequency band gap by considering the steady state response of the periodic system for selected values of $\overline{k}$. Further, an increase in the size of this band gap can be observed with an increase in the value of $\overline{k}$. Figure 3c and d shows the detailed evolution of the ultra-low band gap. (see the increasing size of the shaded region indicated by the arrow lines for $f \in [0\,\text{Hz}, 500\,\text{Hz}]$). Broadly speaking, the introduction of the elastic foundation results in a rightward shift (i.e., higher frequencies) of the frequency-dispersion curves. This behavior differs from that of periodic bars not resting on elastic foundations. The ultra-low-frequency band gap can be linked with the dynamic characteristics of elastic metamaterials that use either local or nonlocal elastic resonators to achieve low-frequency band gaps [4,5,72,73]. In these studies, the elastic resonator appendages create alternative routes for the distribution of elastic energy and manipulate the band structure of the parent structure to introduce a low-frequency band gap. We merely note that the elastic foundation can be regarded as a set of elastic resonators with infinite mass. Hence, the introduction of the elastic foundation in this case, combined with the intrinsic back scattering effects within the periodic beam (resulting in attenuation band gaps), provides alternative routes that lead to the unique band gap characteristics.
- We also observe that while viscoelastic foundations and viscoelastic elements (within periodic structures) both lead to similar dissipation behavior (resulting from the damping effect), they lead to widely different attenuation behavior. We anticipate that this fundamental difference is rooted in the difference in the functional dependence of the elastic energy on either the displacement or strain field. More specifically, in the case of viscoelastic foundation the elastic energy depends directly on the displacement and velocity of the bar, while in the case of viscoelastic elements the energy depends on the strain induced in the bar.[1].

3 Homogenization via fractional-order calculus

In this section, we develop the fractional-order model for the analysis of the periodic bar on the periodic viscoelastic foundation. As a reminder from the previous sections, the overall procedure consists of determining the space–time fractional-order governing equations and obtaining the value of the fractional parameters describing the response of the system. In this regard, the conclusions derived from the parametric studies conducted in Sect. 2 motivate a direct implementation of fractional-order operators to achieve a reduced-order homogenized representation of the periodic system. In order to clearly present the development of the fractional-order model and, more importantly, to highlight the connection and relevance of fractional calculus to the different phenomena observed in the response of the periodic system, we divide the overall procedure into two steps:

- *Step 1* time-fractional operators are used to capture the impact of the viscoelastic foundation on the response of the periodic bar. More specifically, the differ-integral nature of the time factional operators enables a direct route to model memory effects in time resulting from the presence of the viscoelastic foundation. This approach results in the formulation of a time-fractional bi-material bar model that retains the periodic variation of material properties but no longer consists of an explicit viscoelastic foundation. We have schematically illustrated this concept in Fig. 4. As evident from the figure, each section within the original periodic system along with the corresponding foundation element is replaced by a reduced model consisting of a bar with modified (fractional model) properties. Broadly speaking, this can be interpreted as a model-order reduction technique where the impact of the different foundation elements are directly captured within the time-fractional operator and periodic material properties of the fractional bi-material bar. This procedure is analogous to the fractional model-order reduction technique developed in [43] and extends the latter formulation from lumped to continuum level description.
- *Step 2* the time-fractional bi-material bar model, obtained from step 1, is further homogenized by using space-fractional operators. This step results in a space and time-fractional order elastodynamic formulation with uniform material properties that fully captures the response of the bi-material periodic bar attached to the viscoelastic foundation. This final step is illustrated in Fig. 4. This procedure is analogous to the fractional-order homogenization techniques developed in [28,45,46] for periodically stiffened structural elements. We highlight that, in contrast to the aforementioned studies, the present study also accounts for

[1] Recall that for a 1D viscoelastic element the stress and strain (also strain rate) are related as: $\sigma(x) = E\epsilon(x) + E'\dot{\epsilon}(x) \equiv E\mathrm{d}u/\mathrm{d}x + E'\mathrm{d}\dot{u}/\mathrm{d}x$ [13]

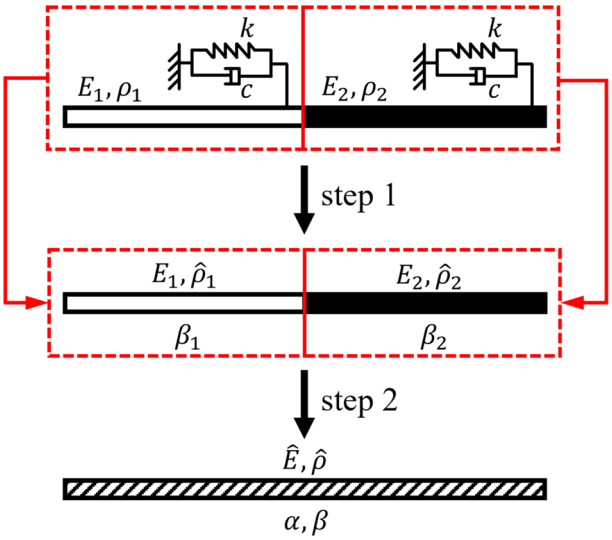

Fig. 4 Two step homogenization via fractional operators. Time-fractional operators are exploited in the first step to capture the viscoelastic foundation and space-fractional operators are further leveraged in the second step to homogenize the space periodic time-fractional bar model

the dissipation resulting from the periodic viscoelastic foundation via the time-fractional operator (in step 1). The most immediate consequence of this extension is reflected in the time-space fractional form of the governing equations.

A detailed discussion of the mathematical formulation underlying the two steps described above is presented in the following two sections. In each section, we also present the inverse strategy to determine the value of fractional-order parameters.

3.1 Step 1: time-fractional bi-material periodic bar model

As mentioned in the introduction to Sect. 3, we develop a time-fractional elastodynamic formulation to capture the impact of the viscoelastic foundation on the response of the periodic bar. Several theoretical [58,74] and experimental [75–78] studies provided direct evidence of the ability of time-fractional operators to capture memory effects and frequency-dependent material properties (such as those typical of viscoelastic materials). Consequently, time-fractional constitutive models have been extensively used in the literature to model viscoelastic behavior [55–57,79,80]. A detailed review of the different fractional-order approaches to viscoelasticity can be found in [59]. Given the extensive literature available on the application of time-fractional differential equations to the modeling of viscoelasticity, we do not focus on the fractional-order mathematics but rather leverage available results to develop the reduced-order model and the inverse strategy.

3.1.1 Constitutive modeling

The extensive evidence showing the ability of time-fractional operators in accurately capturing the underlying physical processes in viscoelastic materials motivates the introduction of the time-fractional operators in the classical governing equations (Eq. (2)) of the periodic bar system. Recall that a fractional-order derivative (say, of order β) can be considered as an interpolation between consecutive integer-order derivatives ($n-1 < \beta < n$; $n \in N^+$) [81]. By following the above considerations, we replace the second-order, first-order, zero-order temporal derivatives of the axial displacement field (that capture the effect of the viscoelastic foundation on each section) on the left-hand side of Eq. (2) by a time-fractional derivative, hence obtaining the following set of time-fractional partial differential equations:

$$\hat{\rho}_i \frac{\partial^{\beta_i} \tilde{u}_i}{\partial t^{\beta_i}} = E_i \frac{\partial^2 \tilde{u}_i}{\partial x^2} \tag{13}$$

where $i = 1 \; \forall \; x \in [-L_1 + N\Delta_\mathrm{L}, N\Delta_\mathrm{L}]$ and $i = 2 \; \forall \; x \in [N\Delta_\mathrm{L}, L_2 + N\Delta_\mathrm{L}]$. The overall procedure is schematically illustrated in Fig. 4 (see the step 1 procedure). In Eq. (13), $\tilde{u}_i$ denotes the axial response of the time-fractional periodic bar. Further, $\beta_i \in (0, 2]$ denotes the time-fractional order and $\hat{\rho}_i$ denotes an effective "fractional density" parameter having units of $[\mathrm{kg}^1\mathrm{m}^{-3}\mathrm{s}^{2-\beta}]$. From a physical perspective, $\hat{\rho}_i$ can be interpreted as a visco-inertial term that simultaneously captures the viscoelastic behavior, induced by the foundation, and the inertia of the periodic system [43,63]. To allow the use of integer-order initial conditions, the fractional-order derivative introduced in Eq. (13) is chosen according to the left-handed Caputo definition:

$$\frac{\mathrm{d}^{\beta_i}\tilde{u}_i}{\mathrm{d}t^{\beta_i}} = {}_{t_0}^{\mathrm{C}}D_t^{\beta_i}\left(\mathrm{e}^{\tilde{\mu}t}\right) = \frac{1}{\Gamma(n_i - \beta_i)}\int_0^t \frac{\mathrm{d}^n\tilde{u}_i(\tau)}{\mathrm{d}\tau^n}(t-\tau)^{n_i-\beta_i-1}\mathrm{d}\tau \tag{14}$$

where $n_i = \lceil \beta_i \rceil$, $\Gamma(\cdot)$ is the Gamma function, τ is a dummy variable of integration, and t is the independent variable of integration that in this case takes the physical meaning of time.

3.1.2 Inverse strategy

In order to determine the fractional parameters, β_i and $\hat{\rho}_i$, we need the dispersion characteristics of the time-fractional governing equations in Eq. (13) in order to follow the inverse strategy outlined previously. For this purpose, in analogy with the approach in Sect. 2, we first consider the solution of the time-fractional governing equations. Since the spatial heterogeneity of the bar is retained in this model, the Floquet theorem can be used to derive the solution to Eq. (13). Consequently, the axial displacement of each section within the time-fractional bar can be chosen as:

$$\tilde{u}_i(x,t) = \tilde{U}_i(x)\mathrm{e}^{\mathrm{j}\tilde{\mu}x}\mathrm{e}^{\mathrm{j}\omega t} \tag{15}$$

where $\tilde{U}_i(x)$ is a periodic function with period Δ_L and $\tilde{\mu}$ denotes the Floquet wavenumber of the time-fractional periodic bar. To obtain the dispersion relation for the time-fractional wave equation in Eq. (13), we assume $t_0 = 0$ and $t \to \infty$ such that [82] (also see the supplementary material (SM) for more detailed derivation):

$${}_{t_0}^{\mathrm{C}}D_t^{\beta_i}\left(\mathrm{e}^{\mathrm{j}\omega t}\right) = {}_{0}^{\mathrm{C}}D_t^{\beta_i}\left(\mathrm{e}^{\mathrm{j}\omega t}\right)\big|_{t\to\infty} = (\mathrm{j}\omega)^{\beta_i}\mathrm{e}^{\mathrm{j}\omega t} \tag{16}$$

Substituting the above ansatz into Eq. (13), we obtain that:

$$\frac{\partial^2\tilde{U}_i}{\partial x^{*2}} + 2\mathrm{j}\tilde{\mu}\frac{\partial\tilde{U}_i}{\partial x^*} + \left[(\mathrm{j}\tilde{\mu})^2 - \frac{(\mathrm{j}\omega)^{\beta_i}\hat{\rho}_i}{E_i}\right]\tilde{U}_i = 0 \tag{17}$$

Note that the limit condition $t \to \infty$ is introduced to simplify the derivation of time-fractional Caputo derivative. When $t < \infty$ is a finite value, Caputo derivative of an exponential function returns Mittag–Leffler functions, not the function with exponential kernels shown in Eq. (16) [82]. We highlight that it is physically compatible to assume $t \to \infty$ when deriving the wave dispersion relation and the steady-state solution simply because: (1) In the context of the dispersion analysis, we look at the intrinsic (eigenvalue-like) response of the system which is essentially time independent and (2) in the context of steady-state analysis, we ignore the temporal oscillation and therefore the overall response does not depend on time.

The solution of the second-order ordinary differential equation derived in Eq. (17) is given by:

$$\tilde{U}_i(x) = \tilde{U}_{i1}\mathrm{e}^{(\tilde{\lambda}_i - \mathrm{j}\tilde{\mu})x^*} + \tilde{U}_{i2}\mathrm{e}^{(-\tilde{\lambda}_i - \mathrm{j}\tilde{\mu})x^*} \tag{18}$$

where $\tilde{U}_{i1}$ and $\tilde{U}_{i2}$ are either real or complex constants. Further, $\tilde{\lambda}_i$ is given as:

$$\tilde{\lambda}_i = \sqrt{\frac{(\mathrm{j}\omega)^{\beta_i}\hat{\rho}_i}{E_i}} \tag{19}$$

To ensure that the time-fractional wave equation in Eq. (13) captures the same dynamic behavior given by the fully resolved integer-order wave equation in Eq. (2), it is necessary to enforce the equivalence of their dispersion relations. By comparing Eqs. (5) and (18), it can be found that:

$$\{\tilde{U}_{ij}, \tilde{\lambda}_i, \tilde{\mu}_i\} = \{U_{ij}, \lambda_i, \mu_i\} \tag{20}$$

where $j \in \{1, 2\}$. Substituting the expressions for λ_i and N_i into above equation produces the following expression for the effective fractional density:

$$\hat{\rho}_i = \frac{\mathrm{j}\bar{c}\omega + \bar{k} + (\mathrm{j}\omega)^2\rho_i}{(\mathrm{j}\omega)^{\beta_i}} \equiv \frac{(\bar{k} - \rho_i\omega^2)\cos\left(\frac{\pi}{2}\beta_i\right) + \bar{c}\omega\sin\left(\frac{\pi}{2}\beta_i\right)}{\omega^{\beta_i}} - \frac{(\bar{k} - \rho_i\omega^2)\sin\left(\frac{\pi}{2}\beta_i\right) - \bar{c}\omega\cos\left(\frac{\pi}{2}\beta_i\right)}{\omega^{\beta_i}}\mathrm{j} \tag{21}$$

Note that in Eq. (21), $\hat{\rho}_i$ and β_i represent two unknown quantities. Hence, in order to determine the values of $\hat{\rho}_i$ and β an additional independent condition is required. This second condition is chosen as $\Im(\hat{\rho}_i) = 0$. Note that if the effective fractional density is a complex quantity, then $\Im(\hat{\rho}_i)$ would also contribute to the dissipation in the system, preventing us from distinguishing the specific extent to which $\hat{\rho}_i$ and β_i capture viscoelasticity. However, we require that the fractional-order β_i captures the entire effects of the viscoelastic foundation. To guarantee that $\hat{\rho}_i \in \mathbb{R}$, it is sufficient to enforce that:

$$(\bar{k} - \rho_i\omega^2)\sin\left(\frac{\pi}{2}\beta_i\right) - \bar{c}\omega\cos\left(\frac{\pi}{2}\beta_i\right) = 0 \tag{22}$$

which leads to the following expressions for β_i and $\hat{\rho}_i$:

$$\beta_i = \frac{2}{\pi}\tan^{-1}\left(\frac{\bar{c}\omega}{\bar{k} - \rho_i\omega^2}\right) \tag{23a}$$

$$\hat{\rho}_i = \frac{\bar{k} - \rho_i\omega^2}{\omega^{\beta_i}\cos(\frac{\pi}{2}\beta_i)} = \frac{\bar{c}\omega}{\omega^{\beta_i}\sin(\frac{\pi}{2}\beta_i)} \tag{23b}$$

Remarkably, the condition $\Im(\hat{\rho}_i) = 0$ also ensures that $\beta_i \in \mathbb{R}$, as evident from the expression above. This latter aspect is instrumental in avoiding computational complexities associated with the evaluation of complex valued fractional derivatives (see [28,43,44]). As evident from Eq. (23), both $\hat{\rho}_i$ and β_i are functions of the angular frequency ω. This observation is consistent with the frequency-dependent properties noted for viscoelastic materials. From a different perspective, the fractional-order formulation for the periodic bar results in a variable order β_i, where β_i is a function of the angular frequency ω. In other terms, the derived model allows the underlying formulation to evolve naturally in the frequency domain, guided by the frequency-dependent variable-order law that is presented in Eq. (23a). Note that the overall formulation is still constant-order in the spatial domain. In other terms, the fractional-order that determines the strength of nonlocality (here, resulting from the material heterogeneity) is uniform across the domain of the solid. We refer the interested reader to [23,24] for detailed discussions on a generalized formulation for variable-order elasticity and its practical applications.

The expressions for the fractional model parameters in Eq. (23) allow us to draw insights into the fractional model-order reduction. We evaluate $\beta_1(\omega)$ and $\hat{\rho}_1(\omega)$ for the aluminum-brass periodic bar configuration introduced in Sect. 2, for different combinations of the foundation coefficients. The parametric studies performed here are identical to study 1 and study 2 conducted in Sect. 2.2 and the results are presented in Figs. 5 and 6, respectively. First, note that, in the limiting case when $\bar{k} = \bar{c} = 0$, the time-fractional bar equation given in Eq. (13) reduces exactly to the integer-order governing equations given in Eq. (2) as also evident from the integer-order values for the time-fractional order β_i and the classical values for $\hat{\rho}_i$. Further, a more detailed analysis of the results leads to the following observations on the effect of the foundation coefficients on the fractional model parameters:

- *Impact of* $\bar{c}$ all the fractional model parameters approach the corresponding limiting case result asymptotically, as the frequency (f) increases. As the damping $\bar{c}$ increases, for a given value of f, the effective density $\hat{\rho}_i$ increases while the time-fractional order β_i decreases. These results are consistent with the literature on time-fractional viscoelasticity [55,57,79]. Further, note that in all the cases $\beta_i \in [1, 2]$ hence indicating a dominance of the visco-inertial regime over the viscoelastic regime [63] as well as a hybrid propagation mechanism of the elastic waves in the periodic system [45,57].
- *Impact of* $\bar{k}$ all the fractional model parameters present a non-smooth variation marked by the presence of either a jump (as in β_i) or a cusp (or equivalently, point of inflection, as in $\hat{\rho}_i$ which stands in direct constant to the previous set of results (where $\bar{k} = 0$). From a mathematical perspective, the dispersion curves for $\bar{k} \neq 0$ do not satisfy C^1 continuity, while the dispersion curves for $\bar{k} = 0$ are C^1 continuous. Note that the jump in β_i from $\beta_i = 0$ to $\beta_i = 2$ is expected since the time-fractional order cannot lie in

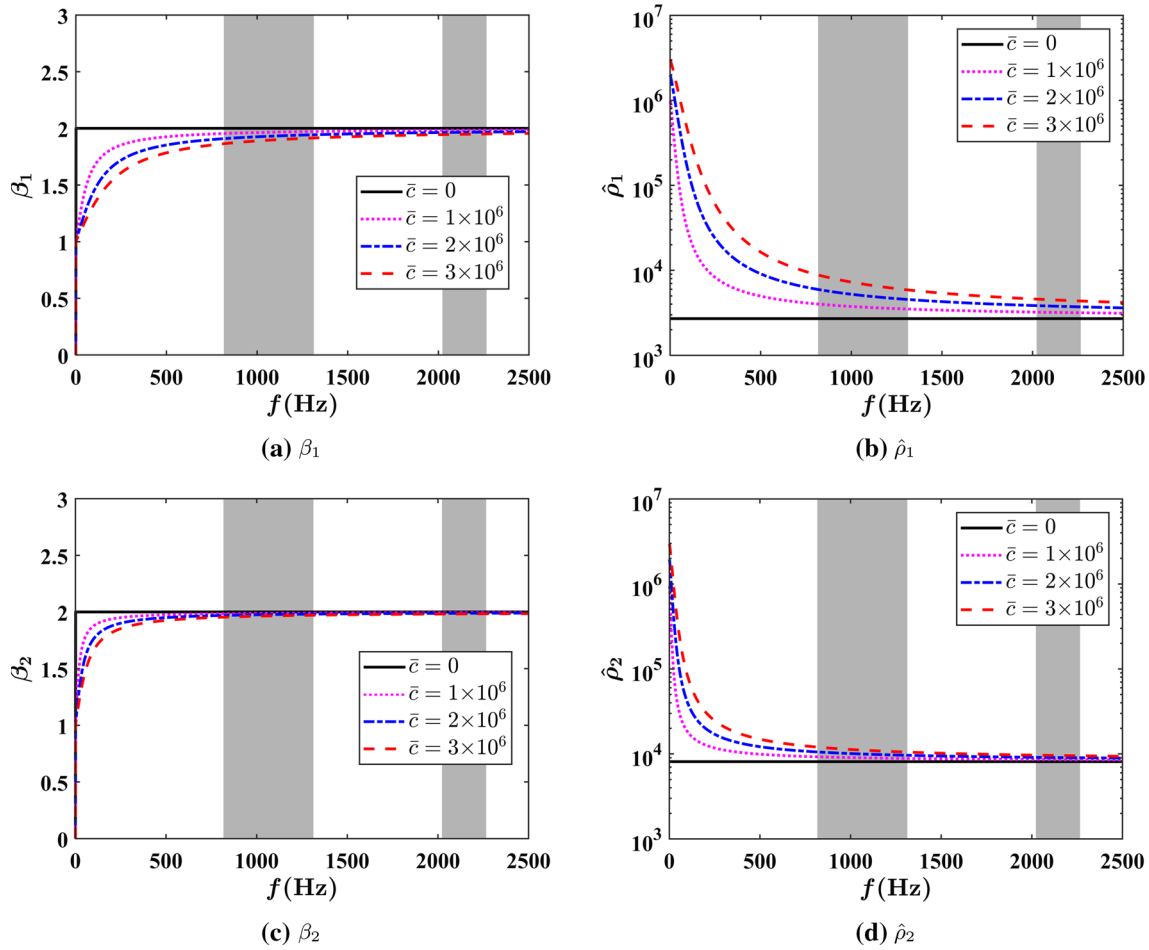

Fig. 5 Curves of the fractional orders β_1, β_2 and the effective fractional densities $\hat{\rho}_1$, $\hat{\rho}_2$ in study 1. **a** and **b** show how β_1 and $\hat{\rho}_1$ change with $\bar{c}$ when $\bar{k} = 0$; **c** and **d** show how β_2 and $\hat{\rho}_2$ change with $\bar{c}$ when $\bar{k} = 0$. Note that β_1 and β_2 have the same trends as f changes. Same conclusion also applies to $\hat{\rho}_1$ and $\hat{\rho}_2$

the interval $(0, 2)$ as it is representative of a dissipative dynamics. Unlike the previous case, there is no damping in the present system and hence, the system is conservative in nature.

3.2 Step 2: Space–time fractional homogeneous bar model

Recall that the differ-integral nature of space-fractional operators enables them to capture nonlocal effects rooted in either material heterogeneity or intentionally nonlocal geometric designs to achieve accurate and computationally efficient descriptions of complex structures at the continuum level [23,28,47]. As an example, space-fractional operators were leveraged in [28,46] to achieve homogenized models that could accurately predict band gaps and spatial attenuation in periodically stiffened structural elements. Similarly, space-fractional operators were also used to accurately capture the response of porous and functionally graded structural elements [23,24]. We merely note that the aforementioned studies did not consider the effect of viscoelastic foundations and, in a more general sense, the interplay between time and space-fractional operators, that is between dissipative and attenuating mechanisms. Nonetheless, we leverage (and combine) this recent progress in space-fractional mechanical models and the formulation developed in step 1 to develop a space–time fractional homogenized bar model. As in the development of step 1, we begin with the constitutive modeling and develop an inverse strategy to derive the space–time fractional model parameters for practical applications.

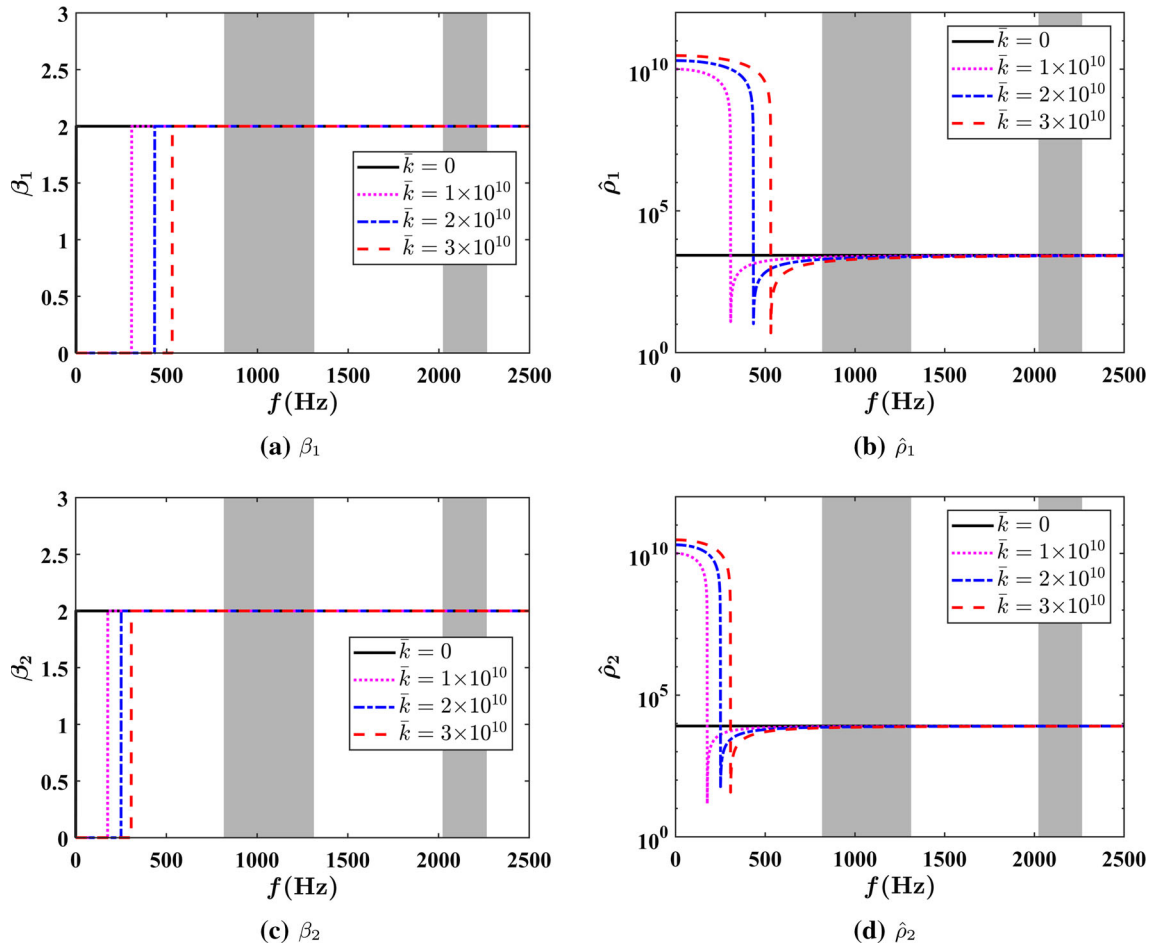

Fig. 6 Curves of the fractional orders β_1, β_2 and the effective fractional densities $\hat{\rho}_1$, $\hat{\rho}_2$ in study 2. **a** and **b** show how β_1 and $\hat{\rho}_1$ change with $\bar{k}$ when $\bar{c} = 0$; **c** and **d** show how β_2 and $\hat{\rho}_2$ change with $\bar{k}$ when $\bar{c} = 0$. Note that β_1 and β_2 have the same trends as f changes. Same conclusion also applies to $\hat{\rho}_1$ and $\hat{\rho}_2$

3.2.1 Constitutive modeling

In this section, in addition to the time-fractional operators in the reduced-order model in Eq. (13), we introduce space-fractional operators to map the bi-material periodic bar to a homogenized material system described by space-fractional constitutive relations. More specifically, the periodic (spatial) variation in the material properties of the bar (in the fully resolved integer-order model or the time-fractional periodic bar model) is no longer retained in the present space–time fractional model. The overall procedure is schematically illustrated in Fig. 4 (see the second step). Based on the space-fractional 1D wave equation proposed in [28] and the time-fractional wave equation used in Sect. 3.1, the space–time fractional wave equation describing the longitudinal displacement is now given by:

$$\hat{\rho}\frac{\partial^{\beta}\tilde{\tilde{u}}}{\partial t^{\beta}} = \hat{E}\frac{\partial^{\alpha}\tilde{\tilde{u}}}{\partial x^{\alpha}} \tag{24}$$

where $\beta \in (0, 2]$ and $\alpha \in (0, 2]$ denote the time and space-fractional order, respectively. $\tilde{\tilde{u}}$ denotes the axial response of the space–time fractional periodic bar. $\hat{E}$ is the effective "elastic modulus" of the fractional homogenized bar and has units of $[\mathrm{kg}^1\mathrm{m}^{\alpha-3}\mathrm{s}^{-2}]$. Further, $\hat{\rho}$ denotes the "effective" density of the space–time fractional homogenized bar, analogous to $\hat{\rho}_i$ in step 1 (see Eq. (13)). Analogous to the time-fractional operator, the space-fractional operator in Eq. (24) is chosen according to the Caputo definition. Note that the Caputo derivative of a constant function is zero [81]. This latter characteristic is critical in ensuring that a translation of the body (or equivalently, the origin of the coordinate system) results in zero strain and stress (that is, the

right-hand side of Eq. (24) is zero). In other terms, the Caputo definition guarantees frame invariance of the space–time fractional-order model [45,83].

3.2.2 Determination of the fractional-order parameters

Similarly to the approach in Sect. 3.1.2, we derive the dispersion characteristics of Eq. (24) to estimate the different parameters for homogenization of the bi-material periodic bar on the viscoelastic foundation. Note that differently from the model in step 1, where we assumed different wave solutions for the two sections and enforced continuity conditions, here we can assume a single wave solution that describes the entire homogenized medium. Consider the following two ansatzes:

$$\tilde{\tilde{u}}(x,t) = \tilde{\tilde{U}} \mathrm{e}^{\mathrm{j}\tilde{\tilde{\mu}}x} \mathrm{e}^{\mathrm{j}\omega t} \tag{25a}$$

$$\tilde{\tilde{u}}(x,t) = \tilde{\tilde{U}} \mathrm{e}^{-\mathrm{j}\tilde{\tilde{\mu}}x} \mathrm{e}^{\mathrm{j}\omega t} \tag{25b}$$

where $\tilde{\tilde{U}}$ is the amplitude of the wave, and $\tilde{\tilde{\mu}}$ denotes the homogenized Floquet wavenumber with its real part $\Re\tilde{\tilde{\mu}} > 0$. Note that, two different space exponential functions $\mathrm{e}^{\mathrm{j}\tilde{\tilde{\mu}}x}$ and $\mathrm{e}^{-\mathrm{j}\tilde{\tilde{\mu}}x}$ are formulated in the first and second ansatz to represent backward and forward propagating waves, respectively. We now evaluate the space-fractional Caputo derivatives in both two cases. Specifically, we consider the periodic bar to be semi-infinite long such that by taking the lower bound to be $-\infty$ and ∞ for backward and forward propagating waves, space-fractional Caputo derivatives with respect to harmonic inputs are given by:

$${}^{\text{L-C}}_{-\infty}D^{\alpha}_{x}\left(\mathrm{e}^{\mathrm{j}\tilde{\tilde{\mu}}x}\right) = (\mathrm{j}\tilde{\tilde{\mu}})^{\alpha}\mathrm{e}^{\mathrm{j}\tilde{\tilde{\mu}}x} \tag{26a}$$

$${}^{\text{L-C}}_{x}D^{\alpha}_{\infty}\left(\mathrm{e}^{-\mathrm{j}\tilde{\tilde{\mu}}x}\right) = (\mathrm{j}\tilde{\tilde{\mu}})^{\alpha}\mathrm{e}^{-\mathrm{j}\tilde{\tilde{\mu}}x} \tag{26b}$$

where the fractional operators ${}_{-\infty}^{\text{C}}D_{x}^{\alpha}(\cdot)$ and ${}_{x}^{\text{C}}D_{\infty}^{\alpha}(\cdot)$ are also called as left-handed and right-handed Liouville–Caputo derivative, respectively, defined as:

$${}^{\text{L-C}}_{-\infty}D^{\alpha}_{x} f(x) = \frac{1}{\Gamma(n-\alpha)} \int_{-\infty}^{x} \frac{\mathrm{d}^n f(\tau)}{\mathrm{d}\tau^n} (x-\tau)^{n-\alpha-1} \mathrm{d}\tau \tag{27a}$$

$${}^{\text{L-C}}_{x}D^{\alpha}_{\infty} f(x) = \frac{(-1)^n}{\Gamma(n-\alpha)} \int_{x}^{\infty} \frac{\mathrm{d}^n f(\tau)}{\mathrm{d}\tau^n} (\tau-x)^{n-\alpha-1} \mathrm{d}\tau \tag{27b}$$

Detailed derivation of Eq. (26) is given in the SM. Similar to the time-fractional case shown in Eq. (16), the space-fractional Caputo derivative of space-harmonic wave inputs also returns in exponential form, therefore simplifies mathematical derivation. Note that the same approach is adopted in [28] to obtain a closed-form analytical solution to space-fractional wave equations. Substituting Eq. (25) into Eq. (24) and using the properties in Eqs. (16, 26), we obtain the dispersion, for both forward and backward propagating waves, as:

$$\tilde{\tilde{\mu}} = -\mathrm{j}\left[\frac{\hat{\rho}(\mathrm{j}\omega)^{\beta}}{\hat{E}}\right]^{\frac{1}{\alpha}} \tag{28}$$

We again match the above dispersion characteristic of the fractional wave equation to Eq. (12) that is:

$$\tilde{\tilde{\mu}} = \mu \tag{29}$$

to enforce equivalence in the dynamics of the homogenized model and of the fully resolved bi-material periodic bar with a viscoelastic foundation. The fractional model has four parameters $\{\beta, \alpha, \hat{\rho}, \hat{E}\}$ that must be determined from the equivalence of the dispersion relation (which provides only a single equation). To determine the values of the four unknown model parameters, we first obtain $\hat{\beta}$ and $\hat{\rho}$ using an additional analysis that involves matching the temporal dynamics, and then estimate $\hat{E}$ and α from the equivalence of the dispersion relations.

To determine β and $\hat{\rho}$, we consider matching the temporal dynamics of the integer and fractional models. For this purpose, we equate the Laplace transforms of the dynamic terms of the integer and space–time fractional

wave equations, that are, the left-hand sides of Eqs. (1) and (24), respectively. The Laplace transforms of the left-hand sides of Eqs. (1) and (24) are given, respectively, by:

$$\mathcal{L}\left(\rho\frac{\partial^2 u}{\partial t^2}+\overline{c}\frac{\partial u}{\partial t}+\overline{k}u\right)=\rho U(s)s^2+\overline{c}U(s)s+\overline{k}U(s) \tag{30a}$$

$$\mathcal{L}\left(\hat{\rho}\frac{\partial^\beta u}{\partial t^\beta}\right)=\hat{\rho}U(s)s^\beta \tag{30b}$$

where ρ denotes the effective density of the periodic bar obtained via the classical rule of mixture approach [25]:

$$\rho=\frac{L_1\rho_1}{L_1+L_2}+\frac{L_2\rho_2}{L_1+L_2} \tag{31}$$

Now, by substituting $s=\mathrm{j}\omega$ and equating the Laplace transforms, we obtain that:

$$\hat{\rho}(\mathrm{j}\omega)^\beta=\rho(\mathrm{j}\omega)^2+\overline{c}(\mathrm{j}\omega)+\overline{k} \tag{32}$$

Note that the functional form of the above expression is identical to Eq. (21) (step 1). This is not surprising since we are, in principle, mapping the system dynamics from the time domain in step 1 to the Laplace domain in the present case. Simplifying Eq. (32) and enforcing $\Im(\hat{\rho})=0$, we obtain:

$$\beta=\frac{2}{\pi}\tan^{-1}\left(\frac{\overline{c}\omega}{\overline{k}-\rho\omega^2}\right) \tag{33a}$$

$$\hat{\rho}=\frac{\overline{k}-\rho\omega^2}{\omega^\beta\cos(\frac{\pi}{2}\beta)}=\frac{\overline{c}\omega}{\omega^\beta\sin(\frac{\pi}{2}\beta)} \tag{33b}$$

Note that above presented results can also be directly obtained from Eq. (23) by assuming that $\hat{\rho}_i$ is equivalent to the effective density presented in Eq. (32) [25].

By using the expressions for β and $\hat{\rho}$ in Eq. (33) within the equivalence of between dispersion relations presented in Eq. (29), we obtain:

$$\hat{E}=\frac{\rho(\mathrm{j}\omega)^2+\overline{c}(\mathrm{j}\omega)+\overline{k}}{(\mathrm{j}\mu)^\alpha} \tag{34}$$

Recall that μ is a complex number in general (particularly, when the frequency is located within a band gap). Upon considering the polar expression $\mu=|\mu|\mathrm{e}^{i\theta}$, where θ denotes the argument of μ, $\hat{E}$ can be simplified as:

$$\hat{E}=\frac{\rho(\mathrm{j}\omega)^2+\overline{c}(\mathrm{j}\omega)+\overline{k}}{|\mu|^\alpha\left[\cos((\theta+\frac{\pi}{2})\alpha)+\mathrm{j}\sin((\theta+\frac{\pi}{2})\alpha)\right]} \tag{35}$$

Again, by imposing $\Im(\hat{E})=0$ we obtain the following closed-form expressions for α and $\hat{E}$:

$$\alpha=\frac{2}{\pi+2\theta}\tan^{-1}\left(\frac{\overline{c}\omega}{\overline{k}-\rho\omega^2}\right) \tag{36a}$$

$$\hat{E}=\frac{\overline{k}-\rho\omega^2}{|\mu|^\alpha\cos(\theta\alpha)}=\frac{\overline{c}\omega}{|\mu|^\alpha\sin(\theta\alpha)} \tag{36b}$$

As expected, the fractional model parameters and the effective material properties are a function of frequency. Further, analogous to the inverse strategy outlined for step 1, imposing $\Im(\hat{E})=0$ ensures that both α and $\hat{E}$ are real valued in nature. The real valued nature of α is in contrast to the study conducted in [28], where a complex valued α was obtained to describe the attenuation band gaps and space-fractional dynamics of the periodic bar. We will discuss this aspect in more detail in the parametric study presented below.

We repeat the parametric studies performed previously in Sect. 3.1.2 to analyze the impact of the foundation parameters ($\overline{k}$ and $\overline{c}$) on the fractional model parameters. The results are presented in Figs. 7 and 8 for study

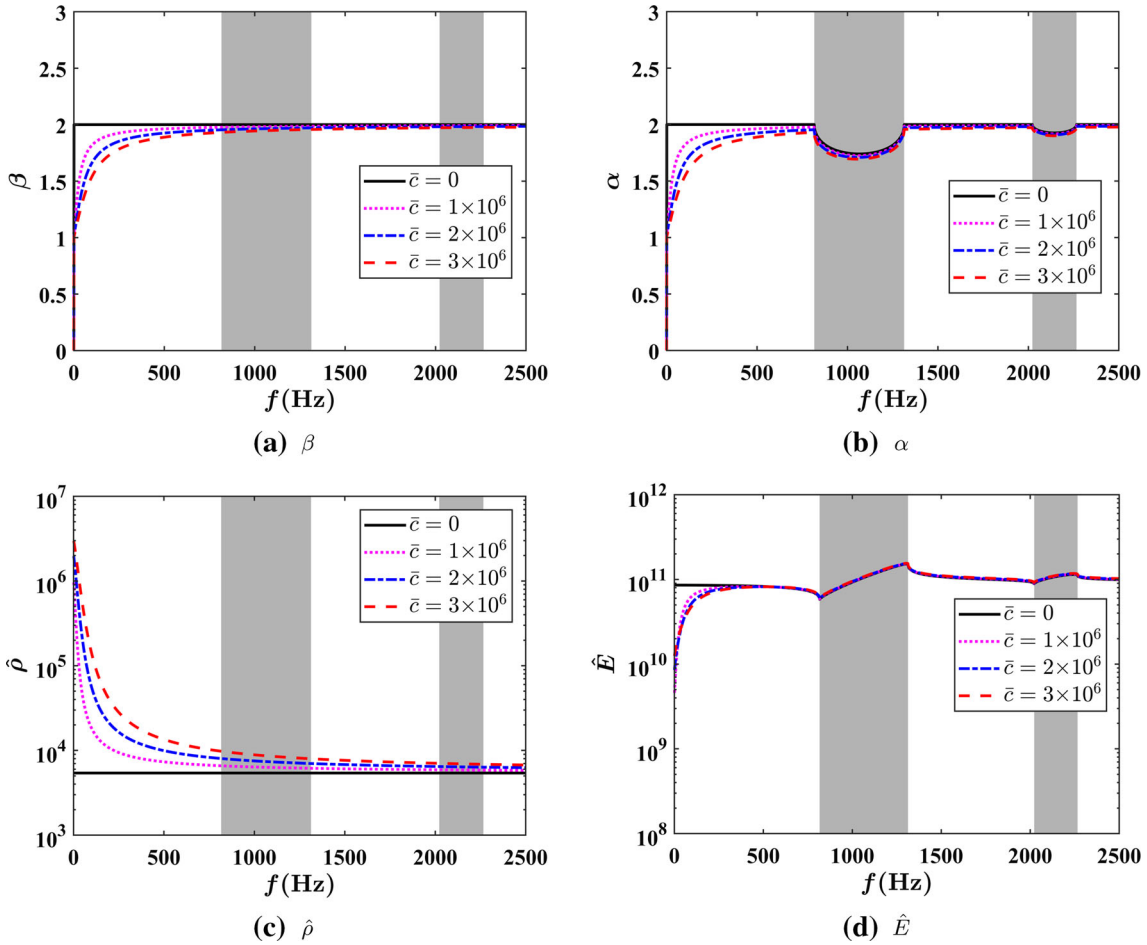

Fig. 7 Results showing how the time-fractional order β, the space-fractional order α, the effective fractional density $\hat{\rho}$, and the effective fractional modulus $\hat{E}$ vary with the frequency f in study 1

1 and 2, respectively. As evident from the results, the conclusions noted on the impact of $\overline{c}$ and $\overline{k}$ on the time-fractional order and effective density in the step 1 model directly extend to the step 2 time-fractional order and effective density parameters. Hence, in the following we only discuss the impact of the foundation parameters on the space-fractional order α and on the effective modulus of elasticity $\hat{E}$. In this regard, note that the values of α and $\hat{E}$ vary significantly within the dispersion band gap indicating a shift in the underlying transport process from being propagating to attenuating in nature. This is more clearly evident from study 2, where we observe that $\alpha \in \{0, 2\}$ in the propagating bands (indicating a classical wave propagation), while $\alpha \in (1.5, 2)$ in the band gaps (indicating anomalous propagation characteristic of attenuating solids [45]. We merely note that the presence of damping leads to an asymptotic approach to the limiting case (as also seen in step 1). On the other hand, note that the presence of band gaps has no effect on the values of the time-fractional order and the effective density (as also the case in step 1 model). This is expected since the presence of band gaps is a direct result of the spatial periodicity of the system which is captured via the space-fractional component of the overall fractional-order homogenized model.

Note that, in the limiting case of $\overline{k} = 0, \overline{c} = 0$ (that is, in the absence of the viscoelastic foundation), and when the angular frequency is within the band pass regime, $\alpha = \beta = 2$ as expected. For this combination of the orders, it can be shown using Eqs. (33, 36) that the effective speed of pressure waves in the bar, given by:

$$\hat{v} = \sqrt{\frac{\hat{E}}{\hat{\rho}}} = \frac{\omega}{\mu} \tag{37}$$

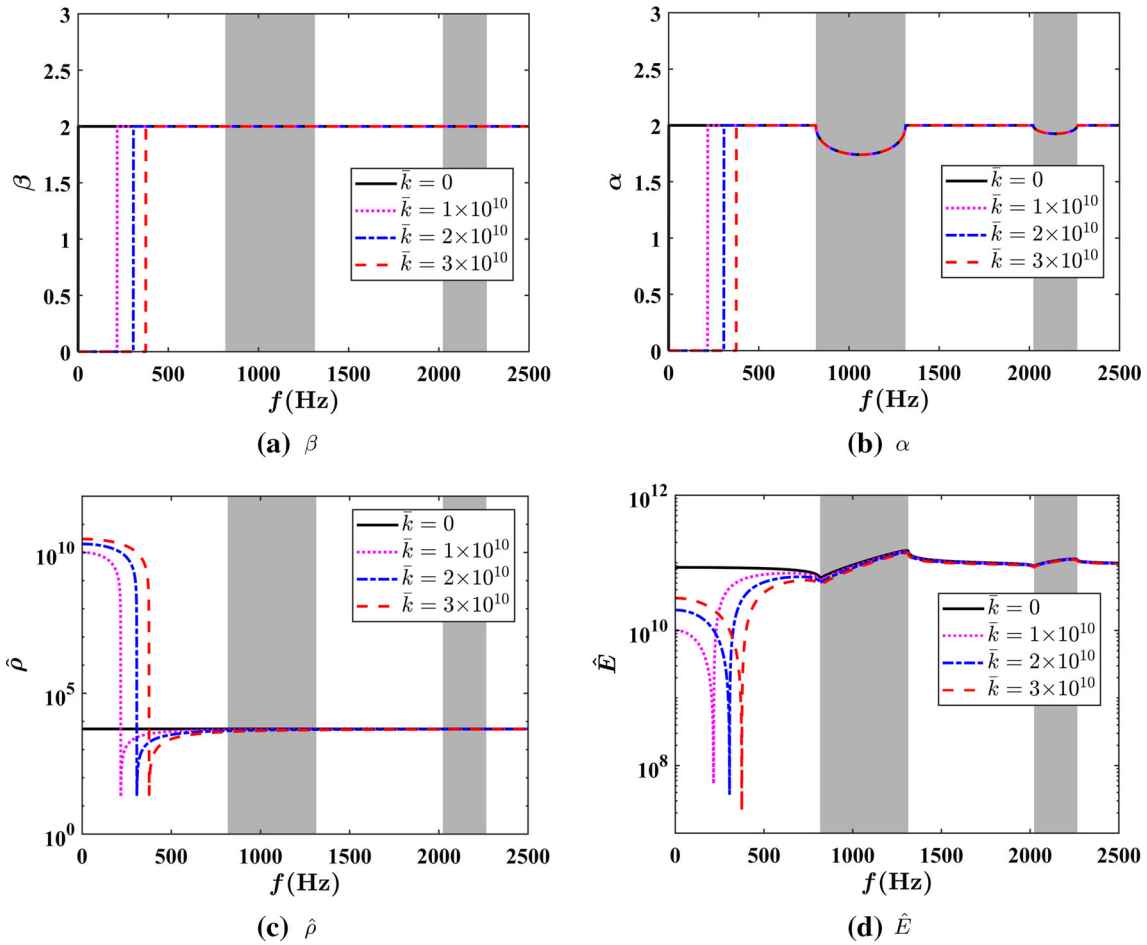

Fig. 8 The zero orders correspond with ultra-low band gap phenomenon. Results showing how the time-fractional order β, the space-fractional order α, the effective fractional density $\hat{\rho}$, and the effective fractional modulus $\hat{E}$ vary with the frequency f in study 2. Note that the four parameters vary drastically within the ultra-low band gap imposed by $\overline{k}$

is consistent with classical predictions [25]. We note also that, under the previous condition ($\overline{k} = 0, \overline{c} = 0$), the values of α, β, and $\hat{v}$ are in exact agreement with the results obtained in the fractional-order homogenization technique proposed in [28]. However, in the more general case, when either $\overline{k} \neq 0$ or $\overline{c} \neq 0$ the results presented in this study differ from the predictions in [28]. More specifically, for the case when the angular frequency is located within a band gap, the space-fractional order α is complex valued in [28] while it is real valued in the present approach. While the approach presented in [28] is still valid, it was pointed out that the use of complex-order fractional derivatives has some drawbacks leading to computational inaccuracies and instabilities.

4 Numerical simulations and validation

In this section, we perform two parametric studies (different from the previously defined study 1 and study 2) to validate the two different fractional-order homogenized models developed for the periodic bar attached to a longitudinal viscoelastic foundation. In the first study, we analyze the effect of the excitation frequency on the steady-state response of the system and in the second study, we analyze the effect of the foundation coefficients on the steady-state response. In all the cases, we consider only the section of the infinite periodic system in the positive x-axis and apply a forcing condition consisting of a sinusoidal axial displacement of unit magnitude at $x = 0$. In each study, we validate the fractional model prediction against the corresponding

integer-order solution. Note that the analytical expressions for the steady-state response of the different models were presented previously while deriving the corresponding dispersion characteristics.

First, we simulate and compare the dynamic response of the periodic system by using the different integer- and fractional-order models for three different excitation frequencies: 100 Hz, 500 Hz, and 1000 Hz. The results of this study are presented in Fig. 9. In each case, we first simulate the response of the periodic bar with a purely viscous foundation ($\overline{k} = 0$ and $\overline{c} = 1\times10^{6}$) and then with a purely elastic foundation ($\overline{k} = 1\times10^{10}$ and $\overline{c} = 0$). First, Fig. 9a reveals a spatially decaying response at $f = 100$ Hz (a frequency value that lies within the low-frequency band gap). Next, as evident from Fig. 9, the match between the fully resolved integer-order model and the developed fractional-order model is excellent for all cases. The root-mean-square-error (RMSE) for the fully fractional (space–time fractional model in step 2) in Fig. 9 is 0.0137, 0.0086, 0.0324, 0.1042, 0.0063, and 0.0056, respectively, for subplots (a) to (f) in Fig. 9. Note that the RMSE of the fractional solution u_i^f with respect to the reference solution u_i is evaluated by:

$$\mathrm{RMSE}\left(u_i^f\right) = \left[\frac{1}{\mathbb{N}}\sum_{i=1}^{\mathbb{N}}\left(u_i^f - u_i\right)^2\right]^{1/2} \tag{38}$$

where $\mathbb{N}$ denotes the number of points used in the spatial discretization of the periodic system, and $u_i^f = \tilde{u}$ for the step 1 fractional solution and $u_i^f = \tilde{\tilde{u}}$ for the step 2 fractional solution. The simulation results indicate that under the variation of wave frequency, both time-fractional and space–time fractional solutions are in great agreement with the reference integer-order solution. The attenuation in the wave amplitude as well as the wave phase is well captured via the fractional-order homogenized model. Further analysis leads to the following discussions:

- Steady-state wave response is more sensitive to changes in the elastic foundation due to its ability of creating very low-frequency band gaps. When frequency f is in a band gap ($f = 100$ Hz and $f = 1000$ Hz), the displacement error is much smaller than the case when f is in a pass band ($f = 500$ Hz). This is due to the fact that the decaying waves in frequency band gaps (the low-frequency band gap created by elastic foundation and the high-frequency band gap created by material periodicity) can reduce the magnitude of scattering effects that occur at periodic material interfaces. For relatively low frequencies shown here ($f = 100$ Hz), the fractional-order homogenization results match the integer-order solutions fairly well and almost exactly in the band gaps. However, for higher frequencies and particularly within pass band regimes ($f = 500$ Hz, where the wavelength is approximately less than two times the length of the unit cell), the accuracy of the homogenization process tends to reduce (reflected in the RMSE values) since the response is increasingly dominated by scattering effects occurring at the interfaces between different materials.
- Damping effects due to a purely viscous foundation are well captured by the fractional-order model. Given that $\Im(\mu) \neq 0$ holds when $\overline{c} > 0$ (see Fig. 3), waves decay at all frequencies due to energy dissipation. While this characteristic is insensitive to the input frequency, amplitude and phase are not. Changes in decay patterns with different input frequencies are shown in Fig. 9a, c and e. Besides the external damping effects, wave decay patterns are also affected by material periodicity. Note that when frequency $f = 100$ Hz, waves decay in both the purely elastic case and the purely viscous case, but show different amplitude and phase (see Fig. 9a, b). This indicates that when $f = 100$ Hz, wave propagation is primarily affected by the external viscoelastic foundations, not material periodicity. In contrast with the above discussion, when frequency $f = 1000$ Hz, band gap exists in both the purely elastic case and the purely viscous case (due to material periodicity) such that amplitude and phase of wave responses are very close (see Fig. 9e, f), regardless of the foundation type. This indicates that when $f = 1000$ Hz, wave propagation is dominated by scattering effects occurring at periodic material interfaces, not external viscoelastic foundations.

We conclude with a parametric study on the impact of the viscoelastic coefficients $\overline{k}$ and $\overline{c}$ on the steady state response of the periodic system for a fixed value of the excitation frequency. The results of this study are presented in Fig. 10a and b for the integer-order model, in Fig. 10c and d for the time-fractional model, and in Fig. 10e and f for the space–time fractional model. As evident from the results, the value of $\overline{c}$ does not affect significantly the wave phase. On the other hand, in the study 2 case, the period and phase of the 1D wave vary for different values of $\overline{k}$. We immediately observe that this phenomenon coincides with the dispersion curves presented in Fig. 3c. Note that due to the increase of $\overline{k}$, $\Re(\mu)$ decreases and eventually leads to the increase of wave period. We highlight that this phenomenon is in fact also consistent with general observations in the

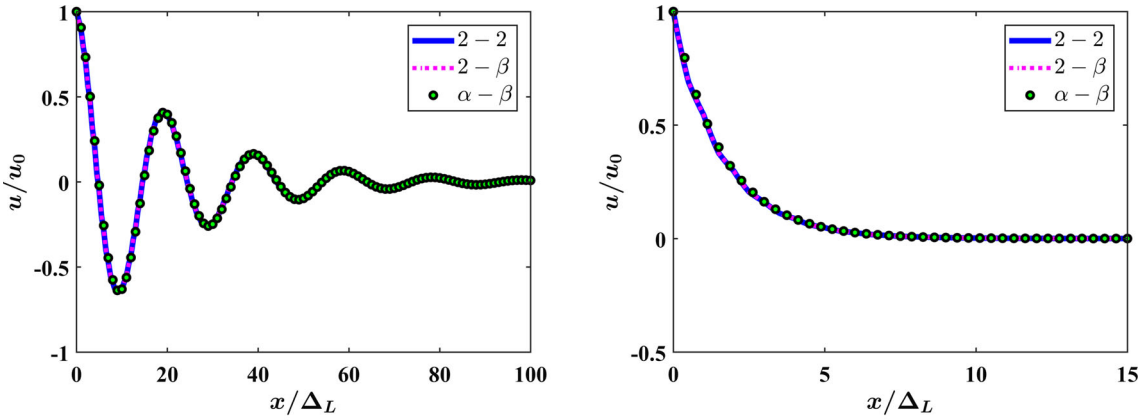

(a) $f = 100\text{Hz}$, $\overline{k} = 0$, $\overline{c} = 1\times10^{6}$, $L = 200\text{m}$ **(b)** $f = 100\text{Hz}$, $\overline{k} = 1\times10^{10}$, $\overline{c} = 0$, $L = 30\text{m}$

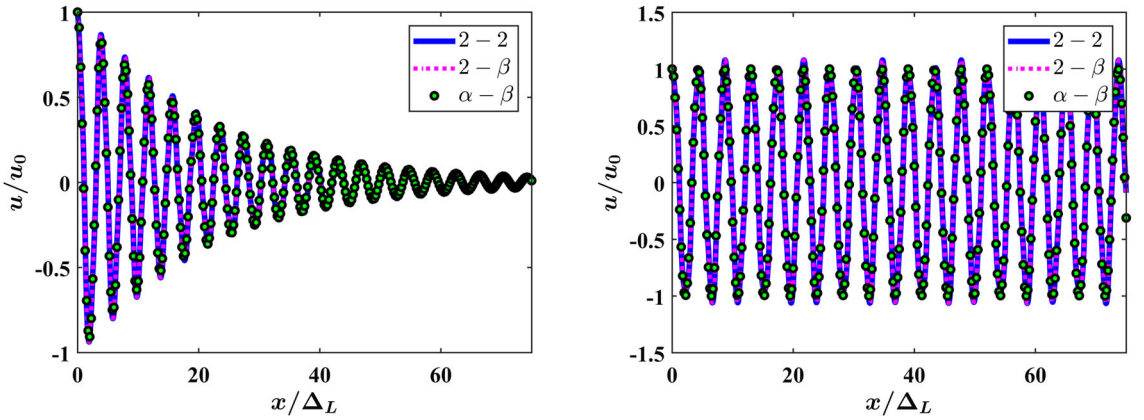

(c) $f = 500\text{Hz}$, $\overline{k} = 0$, $\overline{c} = 1\times10^{6}$, $L = 150\text{m}$ **(d)** $f = 500\text{Hz}$, $\overline{k} = 1\times10^{10}$, $\overline{c} = 0$, $L = 150\text{m}$

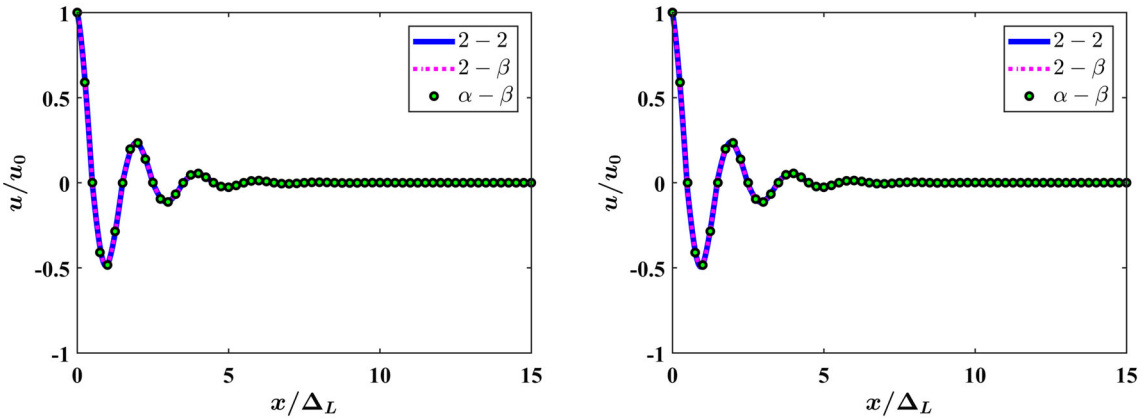

(e) $f = 1000\text{Hz}$, $\overline{k} = 0$, $\overline{c} = 1\times10^{6}$, $L = 30\text{m}$ **(f)** $f = 1000\text{Hz}$, $\overline{k} = 1\times10^{10}$, $\overline{c} = 0$, $L = 30\text{m}$

Fig. 9 Steady-state responses of three wave equations under parametric study of f: Legends formatted "$t_d - x_d$" indicate the wave equation with order t_d for the time derivative and order x_d for the space derivative; Elastic and damping coefficients for (**a**), (**c**), and (**e**) are set as $\overline{k} = 0$ and $\overline{c} = 1\times10^{6}$ (corresponding to study 1); Elastic and damping coefficients for (**b**), (**d**), and (**f**) are set as $\overline{k} = 1\times10^{10}$ and $\overline{c} = 0$ (study 2). Δ_{L} is the length of unit cell before homogenization

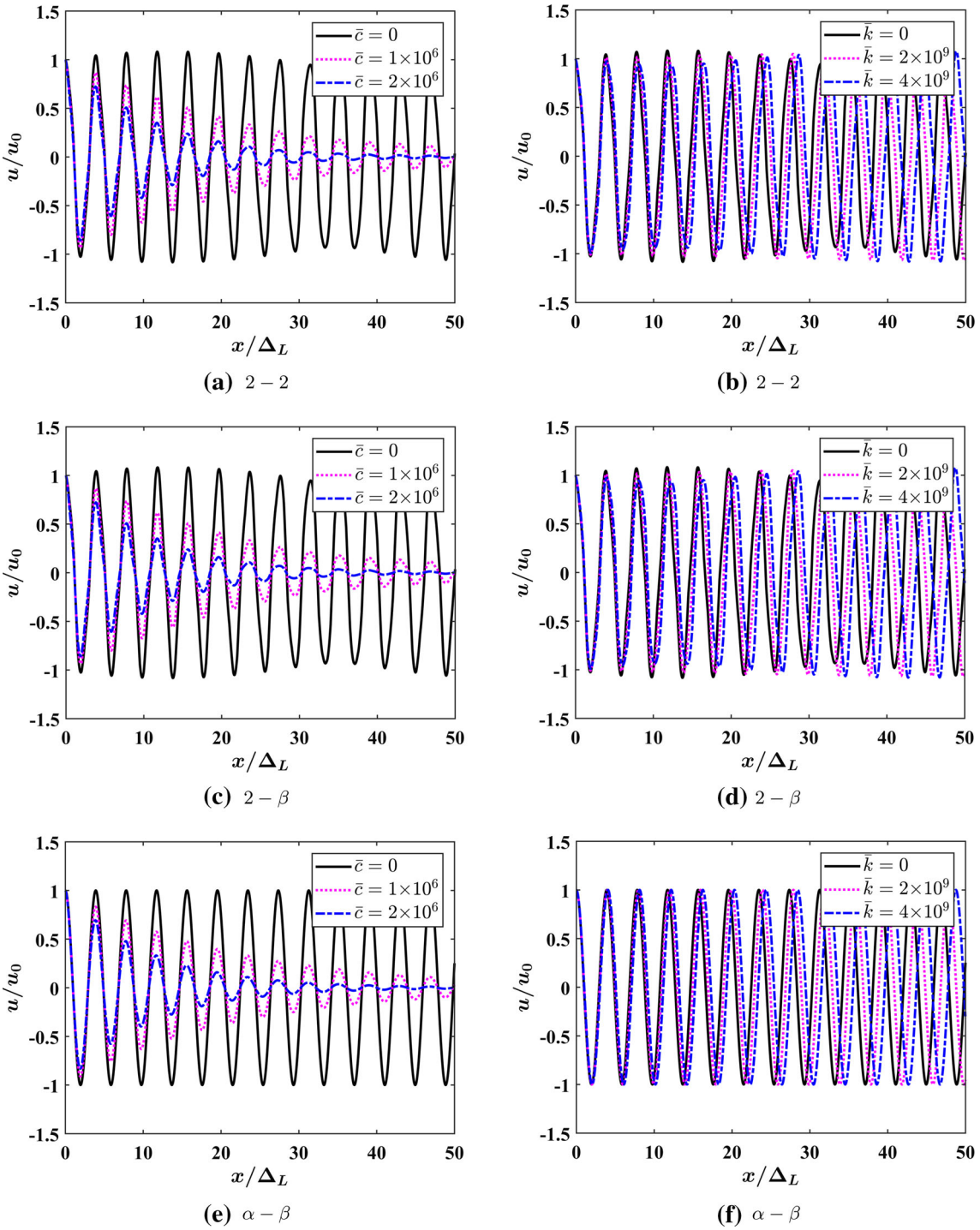

Fig. 10 Steady-state responses of three wave equations under parametric study of $\bar{k}$ and $\bar{c}$: **a**, **c**, and **e** show results for study 1; **b**, **d**, and **f** show the results for study 2. Subcaptions formatted "$t_d - x_d$" indicate wave equation with order t_d for the time derivative and order x_d for the space derivative. Note that $f = 500\,\text{Hz}$ is fixed for both study 1 and study 2. The length of unit cell Δ_L is used to nondimensionalize x in space

classical mass-spring-damper model [84]. For the fractional models, irrespective of the value of $\overline{c}$ change, the two homogenized fractional-order wave equations always produce responses having the same period and phase. We merely note that this observation can be also substantiated by Fig. 3a in which $\Re(\mu)$ does not vary with $\overline{c}$ when $f = 500\,\text{Hz}$. Again, as for the previous set of parametric studies, a very low degree of mismatch is noted in the magnitude of the displacement response. The RMSE for the fully fractional model are 0.0959, 0.0395, 0.0256, and 0.0197 for the case when $\overline{k} = 0$ (see Fig. 10e) and 0.0959, 0.0969, 0.0980, and 0.0997 for the case when $\overline{c} = 0$ (see Fig. 10f). From visual inspection and RMSE values, we confirm that the results between the integer model and the two fractional models are in good agreement, irrespective of the specific combination of the foundation coefficients.

The different parametric studies conducted above establish concretely that the space-fractional model can capture very effectively the attenuation associated with band gaps induced by the spatial periodicity of the bar, while the time-fractional model captures the viscoelastic behavior (by representing the dissipation with a single time-fractional derivative instead of a multiple spring and damping elements). These characteristics make fractional models more attractive than corresponding integer-order representations.

5 Conclusions

This paper proposed a homogenization technique for one-dimensional periodic systems based on fractional-order operators in both time and space. The study generalizes previous fractional homogenization techniques by considering elastic wave propagation in 1D periodic bars resting on a viscoelastic foundation. The system being considered encompasses periodicity in both the main waveguide (i.e., different materials) and in the supports (i.e., periodic stiffening and damping elements), hence providing a very general configuration for the study of conservative and non-conservative 1D periodic media. It also allows accounting for periodicity in either the stiffness or the damping distributions, hence effectively providing a generalized model for the analysis of periodic viscoelastic inhomogeneous systems. The analysis of the dispersion relations shows that besides the classical Bloch wave dispersion behavior, phenomena including very low-frequency band gaps and wave dissipation are observed and carefully linked to the different periodic elements of the design. In order to obtain a homogenized model able of capturing the effect of the original heterogeneous composition of the system on the wave propagation behavior, space-fractional and time-fractional operators were introduced. Based on this approach, two different fractional-order models were proposed based on time-fractional and time-space fractional partial differential equations. By matching the dispersion behavior predicted by the fractional equations to that of the initial (fully resolved) integer-order model, the values of the fractional orders and of the effective parameters in the fractional homogenized models were obtained. As part of this process, we also developed an approach to obtain real-valued fractional orders, as opposed to complex fractional orders obtained in previous methodologies. This approach helped removing complexities and instabilities in the numerical evaluation, as well as clarifying the physical interpretation of the different terms of the model. Numerical simulations clearly indicated the outstanding potential of fractional homogenization techniques by capturing very accurately the wave propagation behavior of the original heterogeneous system. Even more notable is the ability of the method to capture the response within the low-order band gaps (that is in the transition region between long and short wavelength dominated behavior), a characteristic not available in traditional homogenized models.

Acknowledgements The authors gratefully acknowledge the financial support of the National Science Foundation (NSF) under grants MOMS #1761423, and the Defense Advanced Research Project Agency (DARPA) under grant #D19AP00052. J.P.H. acknowledges the financial support of the National Defense Science and Engineering Graduate Fellowship (NDSEG). S.P. acknowledges the financial support of the School of Mechanical Engineering, Purdue University, through the Hugh W. and Edna M. Donnan Fellowship. Any opinions, findings, and conclusions or recommendations expressed in this material are those of the author(s) and do not necessarily reflect the views of the National Science Foundation. The content and information presented in this manuscript do not necessarily reflect the position or the policy of the government. The material is approved for public release; distribution is unlimited.

Declarations

Conflict of interest The authors declare no competing interest.

References

1. Craster, R.V., Guenneau, S.: Acoustic Metamaterials: Negative Refraction, Imaging, Lensing and Cloaking, vol. 166. Springer, Berlin (2012)
2. Hussein, M.I., Leamy, M.J., Ruzzene, M.: Dynamics of phononic materials and structures: historical origins, recent progress, and future outlook. Appl. Mech. Rev. **66**, 38 (2014)
3. Trainiti, G., Ruzzene, M.: Non-reciprocal elastic wave propagation in spatiotemporal periodic structures. New J. Phys. **18**, 083047 (2016)
4. Zhu, H., Patnaik, S., Walsh, T.F., Jared, B.H., Semperlotti, F.: Nonlocal elastic metasurfaces: enabling broadband wave control via intentional nonlocality. Proc. Natl. Acad. Sci. **117**, 26099–26108 (2020)
5. Nair, S., Jokar, M., Semperlotti, F.: Nonlocal acoustic black hole metastructures: achieving broadband and low frequency passive vibration attenuation. Mech. Syst. Signal Process. **169**, 108716 (2022)
6. Ao, X., Chan, C.T.: Far-field image magnification for acoustic waves using anisotropic acoustic metamaterials. Phys. Rev. E **77**, 025601 (2008)
7. Zhang, S., Xia, C., Fang, N.: Broadband acoustic cloak for ultrasound waves. Phys. Rev. Lett. **106**, 024301 (2011)
8. Zhu, H., Semperlotti, F.: Metamaterial based embedded acoustic filters for structural applications. AIP Adv. **3**, 092121 (2013)
9. Zhu, H., Semperlotti, F.: Phononic thin plates with embedded acoustic black holes. Phys. Rev. B **91**, 104304 (2015)
10. Miniaci, M., et al.: Design and fabrication of bioinspired hierarchical dissipative elastic metamaterials. Phys. Rev. Appl. **10**, 024012 (2018)
11. Bhattiprolu, U., Bajaj, A.K., Davies, P.: Periodic response predictions of beams on nonlinear and viscoelastic unilateral foundations using incremental harmonic balance method. Int. J. Solids Struct. **99**, 28–39 (2016)
12. Erturk, A., Inman, D.J.: Piezoelectric Energy Harvesting. Wiley, Hoboken (2011)
13. Kerr, A.D.: Elastic and viscoelastic foundation models. J. Appl. Mech. **31**, 491–498 (1964)
14. Yadav, O.P., Vyas, N.S.: Stick-slips and jerks in an SDOF system with dry friction and clearance. Int. J. Non-Linear Mech. **137**, 103790 (2021)
15. Khan, M., Li, B., Tan, K.: Impact load wave transmission in elastic metamaterials. Int. J. Impact Eng. **118**, 50–59 (2018)
16. Yadav, O.P., Balaga, S.R., Vyas, N.S.: Forced vibrations of a spring-dashpot mechanism with dry friction and backlash. Int. J. Non-Linear Mech. **124**, 103500 (2020)
17. Kargarnovin, M., Younesian, D., Thompson, D., Jones, C.: Response of beams on nonlinear viscoelastic foundations to harmonic moving loads. Comput. Struct. **83**, 1865–1877 (2005)
18. Failla, G., Zingales, M.: Advanced materials modelling via fractional calculus: challenges and perspectives. Proc. R. Soc. A **378**, 20200050 (2020)
19. Navarro, E.A., Gimeno, B., Cruz, J.L.: Modelling of periodic structures using the finite difference time domain method combined with the Floquet theorem. Electron. Lett. **29**, 446–447 (1993)
20. Sigalas, M.M., Garcıa, N.: Theoretical study of three dimensional elastic band gaps with the finite-difference time-domain method. J. Appl. Phys. **87**, 3122–3125 (2000)
21. Shi, S., Chen, C., Prather, D.W.: Plane-wave expansion method for calculating band structure of photonic crystal slabs with perfectly matched layers. J. Opt. Soc. Am. A **21**, 1769–1775 (2004)
22. Nemat-Nasser, S.: General variational methods for waves in elastic composites. J. Elast. **2**, 73–90 (1972)
23. Patnaik, S., Jokar, M., Semperlotti, F.: Variable-order approach to nonlocal elasticity: theoretical formulation, order identification via deep learning, and applications. Comput. Mech. **69**, 267–298 (2022)
24. Patnaik, S., Jokar, M., Ding, W., Semperlotti, F.: On the role of the microstructure in the deformation of porous solids (2022). arXiv preprint arXiv:2202.06750
25. Mei, J., Liu, Z., Wen, W., Sheng, P.: Effective dynamic mass density of composites. Phys. Rev. B **76**, 134205 (2007)
26. Manevitch, L.I., Andrianov, I.V., Oshmyan, V.G.: Mechanics of Periodically Heterogeneous Structures. Springer, Berlin (2013)
27. Craster, R.V., Kaplunov, J., Pichugin, A.V.: High-frequency homogenization for periodic media. Proc. R. Soc. A Math. Phys. Eng. Sci. **466**, 2341–2362 (2010)
28. Hollkamp, J.P., Sen, M., Semperlotti, F.: Analysis of dispersion and propagation properties in a periodic rod using a space-fractional wave equation. J. Sound Vib. **441**, 204–220 (2019)
29. Andrianov, I.V., Bolshakov, V.I., Danishevskyy, V.V., Weichert, D.: Higher order asymptotic homogenization and wave propagation in periodic composite materials. Proc. R. Soc. A Math. Phys. Eng. Sci. **464**, 1181–1201 (2008)
30. Chatterjee, A.: Asymptotic solution for solitary waves in a chain of elastic spheres. Phys. Rev. E **59**, 5912 (1999)
31. Ramírez-Torres, A., et al.: Three scales asymptotic homogenization and its application to layered hierarchical hard tissues. Int. J. Solids Struct. **130**, 190–198 (2018)
32. Goda, I., Ganghoffer, J.-F.: 3d plastic collapse and brittle fracture surface models of trabecular bone from asymptotic homogenization method. Int. J. Eng. Sci. **87**, 58–82 (2015)
33. Huang, Y., Yan, D., Yang, Z., Liu, G.: 2d and 3d homogenization and fracture analysis of concrete based on in-situ x-ray computed tomography images and monte carlo simulations. Eng. Fract. Mech. **163**, 37–54 (2016)
34. Ramírez-Torres, A., et al.: An asymptotic homogenization approach to the microstructural evolution of heterogeneous media. Int. J. Non-Linear Mech. **106**, 245–257 (2018)
35. Fish, J., Yang, Z., Yuan, Z.: A second-order reduced asymptotic homogenization approach for nonlinear periodic heterogeneous materials. Int. J. Numer. Methods Eng. **119**, 469–489 (2019)
36. Saeb, S., Steinmann, P., Javili, A.: Aspects of computational homogenization at finite deformations: a unifying review from Reuss' to Voigt's bound. Appl. Mech. Rev. **68**, 33 (2016)
37. Kouznetsova, V., Geers, M.G., Brekelmans, W.: Multi-scale second-order computational homogenization of multi-phase materials: a nested finite element solution strategy. Comput. Methods Appl. Mech. Eng. **193**, 5525–5550 (2004)
38. Yvonnet, J.: Computational Homogenization of Heterogeneous Materials with Finite Elements. Springer, Berlin (2019)

39. Moulinec, H., Suquet, P.: A numerical method for computing the overall response of nonlinear composites with complex microstructure. Comput. Methods Appl. Mech. Eng. **157**, 69–94 (1998)
40. Schneider, M., Ospald, F., Kabel, M.: Computational homogenization of elasticity on a staggered grid. Int. J. Numer. Methods Eng. **105**, 693–720 (2016)
41. Le, B., Yvonnet, J., He, Q.-C.: Computational homogenization of nonlinear elastic materials using neural networks. Int. J. Numer. Methods Eng. **104**, 1061–1084 (2015)
42. Lu, X., et al.: A data-driven computational homogenization method based on neural networks for the nonlinear anisotropic electrical response of graphene/polymer nanocomposites. Comput. Mech. **64**, 307–321 (2019)
43. Hollkamp, J.P., Sen, M., Semperlotti, F.: Model-order reduction of lumped parameter systems via fractional calculus. J. Sound Vib. **419**, 526–543 (2018)
44. Hollkamp, J.P., Semperlotti, F.: Application of fractional order operators to the simulation of ducts with acoustic black hole terminations. J. Sound Vib. **465**, 115035 (2020)
45. Patnaik, S., Semperlotti, F.: A generalized fractional-order elastodynamic theory for non-local attenuating media. Proc. R. Soc. A **476**, 20200200 (2020)
46. Patnaik, S., Hollkamp, J.P., Sidhardh, S., Semperlotti, F.: Fractional order models for the homogenization and wave propagation analysis in periodic elastic beams. Meccanica **57**, 1–17 (2021)
47. Szajek, K., Sumelka, W., Bekus, K., Blaszczyk, T.: Designing of dynamic spectrum shifting in terms of non-local space-fractional mechanics. Energies **14**, 506 (2021)
48. Lazopoulos, K.: Non-local continuum mechanics and fractional calculus. Mech. Res. Commun. **33**, 753–757 (2006)
49. Carpinteri, A., Cornetti, P., Sapora, A.: A fractional calculus approach to nonlocal elasticity. Eur. Phys. J. Spec. Top. **193**, 193–204 (2011)
50. Ding, W., Patnaik, S., Semperlotti, F.: Multiscale nonlocal elasticity: a distributed order fractional formulation (2021). arXiv preprint arXiv:2201.01219
51. Szajek, K., Sumelka, W.: Discrete mass-spring structure identification in nonlocal continuum space-fractional model. Eur. Phys. J. Plus **134**, 1–19 (2019)
52. Alvarez-Ramirez, J., Fernandez-Anaya, G., Valdes-Parada, F.J., Ochoa-Tapia, J.A.: A high-order extension for the Cattaneo's diffusion equation. Physica A Stat. Mech. Appl. **368**, 345–354 (2006)
53. Tarasov, V.E.: Fractional Dynamics: Applications of Fractional Calculus to Dynamics of Particles, Fields and Media. Springer, Berlin (2011)
54. Magin, R.L.: Fractional calculus models of complex dynamics in biological tissues. Comput. Math. Appl. **59**, 1586–1593 (2010)
55. Szabo, T.L.: Causal theories and data for acoustic attenuation obeying a frequency power law. J. Acoust. Soc. Am. **97**, 14–24 (1995)
56. Chen, W., Holm, S.: Fractional Laplacian time–space models for linear and nonlinear lossy media exhibiting arbitrary frequency power-law dependency. J. Acoust. Soc. Am. **115**, 1424–1430 (2004)
57. Holm, S., Näsholm, S.P.: A causal and fractional all-frequency wave equation for lossy media. J. Acoust. Soc. Am. **130**, 2195–2202 (2011)
58. Chatterjee, A.: Statistical origins of fractional derivatives in viscoelasticity. J. Sound Vib. **284**, 1239–1245 (2005)
59. Mainardi, F.: Fractional Calculus and Waves in Linear Viscoelasticity: An Introduction to Mathematical Models. World Scientific, Singapore (2010)
60. Patnaik, S., Semperlotti, F.: Modeling contacts and hysteretic behavior in discrete systems via variable-order fractional operators. J. Comput. Nonlinear Dyn. **15**, 10 (2020)
61. Patnaik, S., Semperlotti, F.: Variable-order fracture mechanics and its application to dynamic fracture. NPJ Comput. Mater. **7**, 1–8 (2021)
62. Meng, R., Yin, D., Drapaca, C.S.: Variable-order fractional description of compression deformation of amorphous glassy polymers. Comput. Mech. **64**, 163–171 (2019)
63. Orosco, J., Coimbra, C.F.M.: Variable-order modeling of nonlocal emergence in many-body systems: application to radiative dispersion. Phys. Rev. E **98**, 032208 (2018)
64. Akhavan-Safaei, A., Samiee, M., Zayernouri, M.: Data-driven fractional subgrid-scale modeling for scalar turbulence: a nonlocal les approach. J. Comput. Phys. **446**, 110571 (2021)
65. Suzuki, J.L., Tuttle, T.G., Roccabianca, S., Zayernouri, M.: A data-driven memory-dependent modeling framework for anomalous rheology: application to urinary bladder tissue. Fractal Fract. **5**, 223 (2021)
66. Manconi, E., Sorokin, S.: On the effect of damping on dispersion curves in plates. Int. J. Solids Struct. **50**, 1966–1973 (2013)
67. Wang, Y.-F., Wang, Y.-S., Laude, V.: Wave propagation in two-dimensional viscoelastic metamaterials. Phys. Rev. B **92**, 104110 (2015)
68. Frazier, M.J., Hussein, M.I.: Generalized Bloch's theorem for viscous metamaterials: dispersion and effective properties based on frequencies and wavenumbers that are simultaneously complex. C. R. Phys. **17**, 565–577 (2016)
69. Aladwani, A., Nouh, M.: Mechanics of metadamping in flexural dissipative metamaterials: analysis and design in frequency and time domains. Int. J. Mech. Sci. **173**, 105459 (2020)
70. Aladwani, A., Nouh, M.: Strategic damping placement in viscoelastic bandgap structures: dissecting the metadamping phenomenon in multiresonator metamaterials. J. Appl. Mech. **88**, 021003 (2021)
71. Brillouin, L.: Wave Propagation in Periodic Structures: Electric Filters and Crystal Lattices. Courier Corporation, Chelmsford (2003)
72. Yu, D., Wen, J., Shen, H., Xiao, Y., Wen, X.: Propagation of flexural wave in periodic beam on elastic foundations. Phys. Lett. A **376**, 626–630 (2012)
73. Wang, K., Zhou, J., Xu, D., Ouyang, H.: Lower band gaps of longitudinal wave in a one-dimensional periodic rod by exploiting geometrical nonlinearity. Mech. Syst. Signal Process. **124**, 664–678 (2019)
74. Bagley, R.L., Torvik, P.: A theoretical basis for the application of fractional calculus to viscoelasticity. J. Rheol. **27**, 201–210 (1983)

75. Torvik, P., Bagley, R.: On the appearance of the fractional derivative in the behavior of real materials. J. Appl. Mech. Trans. ASME **51**, 294–298 (1984)
76. Narahari Achar, B., Hanneken, J.: Microscopic formulation of fractional calculus theory of viscoelasticity based on lattice dynamics. Physica Scr. **2009**, 014011–014018 (2009)
77. Mashayekhi, S., Miles, P., Hussaini, M.Y., Oates, W.S.: Fractional viscoelasticity in fractal and non-fractal media: theory, experimental validation, and uncertainty analysis. J. Mech. Phys. Solids **111**, 134–156 (2018)
78. Mashayekhi, S., Hussaini, M.Y., Oates, W.: A physical interpretation of fractional viscoelasticity based on the fractal structure of media: theory and experimental validation. J. Mech. Phys. Solids **128**, 137–150 (2019)
79. Mainardi, F.: The time fractional diffusion-wave equation. Radiophys. Quantum Electron. **38**, 13–24 (1995)
80. Alotta, G., Di Paola, M., Failla, G., Pinnola, F.P.: On the dynamics of non-local fractional viscoelastic beams under stochastic agencies. Compos. Part B Eng. **137**, 102–110 (2018)
81. Diethelm, K.: The Analysis of Fractional Differential Equations. Springer, New York (2004)
82. Garrappa, R., Kaslik, E., Popolizio, M.: Evaluation of fractional integrals and derivatives of elementary functions: overview and tutorial. Mathematics **7**, 407 (2019)
83. Patnaik, S., Sidhardh, S., Semperlotti, F.: Towards a unified approach to nonlocal elasticity via fractional-order mechanics. Int. J. Mech. Sci. **189**, 105992 (2021)
84. Gómez-Aguilar, J., et al.: Modeling of a mass-spring-damper system by fractional derivatives with and without a singular kernel. Entropy **17**, 6289–6303 (2015)